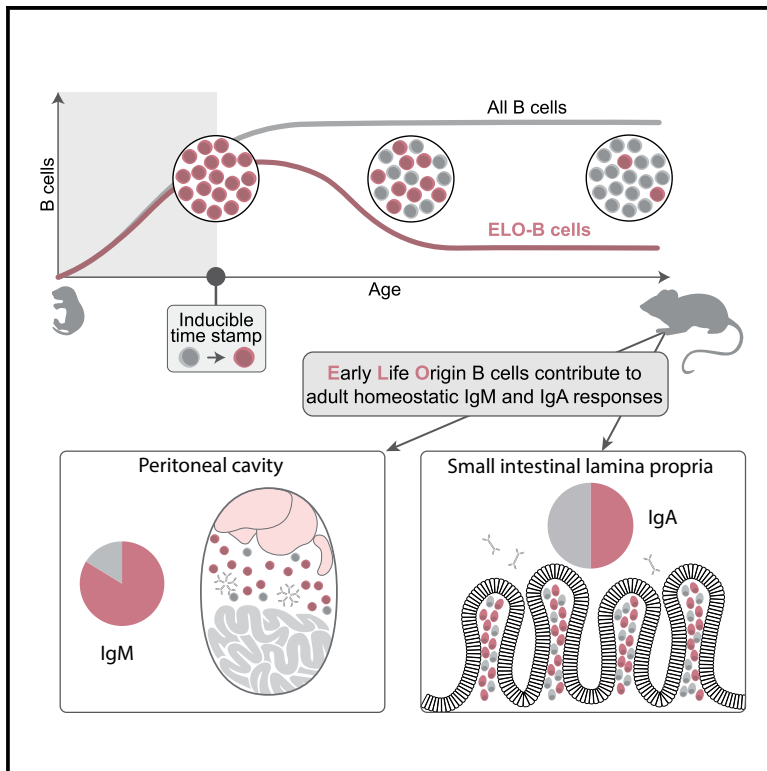


Immunity

A self-sustaining layer of early-life-origin B cells drives steady-state IgA responses in the adult gut

Graphical abstract



Authors

Stefano Vergani,
Konjit Getachew Muleta,
Clément Da Silva, ...,
William Winston Agace, Katharina Lahl,
Joan Yuan

Correspondence

joan.yuan@med.lu.se

In brief

Vergani et al. use time-stamping to examine the relationship between developmental origin and the composition of the adult B cell pool. They find that B cells arising early in life substantially contribute to the IgM and IgA repertoires in unimmunized adult mice. These early-life-origin B cells form a network of self-sustaining IgA memory compartments that archive unique specificities not generated later in life.

Highlights

- Lineage tracing reveals substantial neonatal contribution to the adult B cell pool
- Adult IgA PCs are actively maintained by early-life-induced memory
- Neonatal IgA memory harbors unique recurrent clonotypes not generated in the adult
- B-1a cells and IgA PCs stem from a common progenitor pool during ontogeny

Article

A self-sustaining layer of early-life-origin B cells drives steady-state IgA responses in the adult gut

Stefano Vergani,¹ Konjit Getachew Muleta,³ Clément Da Silva,³ Alexander Doyle,¹ Trine Ahn Kristiansen,¹ Selene Sodini,¹ Niklas Krausse,¹ Giorgia Montano,¹ Knut Kotarsky,³ Joy Nakawesi,³ Hugo Åkerstrand,¹ Stijn Vanhee,¹ Sneh Lata Gupta,¹ David Bryder,² William Winston Agace,^{3,4} Katharina Lahl,^{3,5} and Joan Yuan^{1,6,*}

¹Developmental Immunology Unit, Division of Molecular Hematology, Department of Laboratory Medicine, Lund Stem Cell Center, Lund University, 22242 Lund, Sweden

²Developmental Hematopoiesis Unit, Division of Molecular Hematology, Department of Laboratory Medicine, Lund Stem Cell Center, Lund University, 22242 Lund, Sweden

³Immunology Section, Lund University, Lund 22184, Sweden

⁴Mucosal Immunology Group, Department of Health Technology, Technical University of Denmark, Kemitorvet, 2800 Kgs. Lyngby, Denmark

⁵Section for Experimental and Translational Immunology, Department of Health Technology, Technical University of Denmark (DTU), 2800 Kongens Lyngby, Denmark

⁶Lead contact

*Correspondence: joan.yuan@med.lu.se

<https://doi.org/10.1016/j.immuni.2022.08.018>

SUMMARY

The adult immune system consists of cells that emerged at various times during ontogeny. We aimed to define the relationship between developmental origin and composition of the adult B cell pool during unperturbed hematopoiesis. Lineage tracing stratified murine adult B cells based on the timing of output, revealing that a substantial portion originated within a restricted neonatal window. In addition to B-1a cells, early-life time-stamped B cells included clonally interrelated IgA plasma cells in the gut and bone marrow. These were actively maintained by B cell memory within gut chronic germinal centers and contained commensal microbiota reactivity. Neonatal rotavirus infection recruited recurrent IgA clones that were distinct from those arising by infection with the same antigen in adults. Finally, gut IgA plasma cells arose from the same hematopoietic progenitors as B-1a cells during ontogeny. Thus, a complex layer of neonatally imprinted B cells confer unique antibody responses later in life.

INTRODUCTION

The neonatal immune system is shaped by microbial exposure on the backdrop of ongoing developmental programs (Hornef and Torow, 2020; Kristiansen et al., 2018). This immune education takes place during a restricted “window of opportunity,” which culminates at weaning and has the potential to control long-term immune health and susceptibility to disease later in life (Al Nabhani et al., 2019). Neonatal imprinting affects the long-term functionality of various T cell subsets (Al Nabhani et al., 2019; Constantinides et al., 2019; Melum et al., 2019). However, little is known about the impact of neonatal microbial exposure in shaping the anticipatory adult B cell repertoire.

B-1 cells are a long-lived natural antibody-producing B cell subset (Baumgarth, 2011) and the only B cells in the adult repertoire known to be shaped by early-life antigen exposure (New et al., 2020). They are considered innate-like in function owing to a naturally pre-activated phenotype that is conserved in germ-free conditions and makes them poised for antibody secretion. Transfer experiments have shown that in addition to

IgM, B-1 cells can also reconstitute gut IgA plasma cells (PCs) (Kroese et al., 1989), suggesting that they may be a major source of homeostatic IgA responses. Transplantation of mouse fetal liver (FL), but not adult bone marrow (BM), progenitor cells can efficiently regenerate a CD5+ subset of B-1 (aka B-1a) cells in immunocompromised adult hosts. These findings gave rise to the general consensus that B-1a cells are a distinct lineage of naive B cells primarily of fetal ontogeny and helped fuel the layered immune system hypothesis (Herzenberg and Herzenberg, 1989).

This hypothesis postulates that the complex pool of adult immune cells stem from distinct waves of hematopoiesis early in life and that these ontogenically distinct cell types work in concert to perform the diverse functions of the mammalian immune system. As it pertains to B cells, this idea has been largely tested using transplantation approaches that differ significantly in kinetics from unperturbed hematopoiesis (Busch and Rodewald, 2016). Although such studies unequivocally demonstrate developmental changes in lineage potential intrinsic to hematopoietic stem and progenitor cells (HSPCs), they do not provide

information on the developmental composition of the adult B cell pool in the native context. Indeed, studies on the origin of B-1a cells have measured what transplanted progenitors “can make” rather than what they “do make” *in situ*, leading to contradictory results on the precise window and identity of B-1a cell progenitors during ontogeny (Ghosh et al., 2019). Similarly, the evidence for B-1 cells as a source of gut IgA responses is limited to transfer studies, and the actual contribution to IgA PCs in unperturbed mice remains unknown (Bunker et al., 2015; Kroese et al., 1989).

Here, we employed genetic lineage tracing to investigate the layered formation of the adult B cell compartment, free from pre-conceived notions, during unperturbed organismal development. We discovered that B-1a cells arise during a predominantly postnatal rather than embryonic or fetal window of lymphopoiesis. This window is shared with several other antigen-experienced adult B cell subsets, including gut IgA PCs. Neonatally induced IgA PCs harbor microbiota-reactive clonotypes and are actively maintained by gut chronic germinal center (GC) and memory B cells (MBCs) of early-life origin (ELO). Importantly, neonatal rotavirus (RV) infection recruits IgA memory clonotypes that are distinct from those generated in the adult. Finally, we shed light on the lineage relationship of adult B-1a and IgA PCs using a combination of clonal-tracking approaches.

RESULTS

Time-stamping early-life-origin B cells in the adult

To systematically determine the contribution of early-life lymphopoiesis to the adult B cell pool, we employed tamoxifen (Tam)-inducible Cre-recombinase-mediated *in situ* lineage tracing, which is a powerful approach to interrogate the layered formation of the adult immune system (Ginhoux and Guillemins, 2016; Smith et al., 2018). We took advantage of the *Mb1Cre^{ERT2}* allele (Hobeika et al., 2015) in which CreERT2 expression is driven by the *CD79a* promoter and active from the very first stages of B lineage commitment until terminally differentiated PCs (Sakaguchi et al., 1988; Shi et al., 2015). Therefore, once crossed to the *R26^{fl-STOP-Tom}* reporter strain, Cre expression irreversibly labeled developing and pre-existing B lineage cells at the time of Tam administration with the TdTomato fluorescent protein (Tom+), while leaving subsequent B lineage output from multipotent HSPCs unlabeled (Tom−) (Figure 1A). To validate the efficacy of this “time-stamping” approach, we checked for labeling frequency at 3 days and 3 months following a single dose of Tam administration in 19-day-old juvenile mice (Figure 1B). FACS analysis showed efficient labeling of splenic follicular B (FO-B) and CD5+ peritoneal cavity (PerC) B-1a cells at 3 days after Tam treatment (Figures 1B and S1A). Following a 3-month chase period, the majority of FO-B cells were Tom−, consistent with their expected replacement by newly generated B cells from the BM (Förster and Rajewsky, 1990). In contrast, little influx of unlabeled cells was observed among PerC B-1a cells, in line with their ELO and self-renewing capacity (Kantor et al., 1995). No labeling was detected outside of the B cell lineage at any time following Tam treatment (Figure S1B). Thus, this tracing strategy yields stringent, but likely subsaturated, B cell labeling upon induction and allows for the longitudinal identification of early-origin B cells (Figure 1A).

B-1a cells are efficiently generated by FL but not adult HSPCs, as demonstrated using transplantation approaches (Li et al., 1996). To determine the precise developmental composition of the B-1a cell pool during native hematopoiesis and resolve the window of B-1a origin in unperturbed adult mice, we varied the timing for Tam induction ranging from E17.5 to 5 weeks of age (Figure 1C). Following a 3–4-month chase period, adult PerC and splenic B cell subsets were analyzed for labeling frequency (Figures 1D, 1E, and S1A). Our results demonstrate that while around 20% of B-1a cells become time-stamped *in utero*, a majority acquire labeling postnatally until day 19 (Figure 1D). No additional labeling was detected beyond this time point, indicating an attenuated influx into the long-lived B-1a cell compartment. B-1a cells in adult mice are known to be dominated by self-antigen expanded VH11- and VH12-encoded specificities against the common phospholipid phosphatidyl choline (PtC) (Arnold et al., 1994). Indeed, PtC liposome reactive B cells display a highly similar developmental window (Figure S1C). These findings demonstrate, in contrast to previous transplantation-based studies (Ghosh et al., 2019), that postnatal rather than fetal lymphopoiesis is the numerically predominant source of CD5+ B-1a cells in the unperturbed adult mouse.

Together with B-1a cells, PerC CD5− B-1b cells and splenic marginal zone (MZ) B cells also contribute to the T-independent natural IgM repertoire (Haas et al., 2005; Martin et al., 2001). Interestingly, both populations were enriched for cells that become postnatally time-stamped prior to day 19, demonstrating a shared developmental window (Figures 1D and 1E). In comparison, conventional PerC B-2 cells and splenic FO-B cells displayed low levels (<10%) of early postnatal label retention. These results are consistent with the known ability of innate-like B cells to self-sustain in the absence of BM output (Hao and Rajewsky, 2001; Kantor et al., 1995), whereas FO-B cells are continuously replenished to preserve repertoire diversity.

Extending from these findings, we next investigated the developmental composition of IgM producing BM PCs, which have been linked to innate-like B cell origin (Förster and Rajewsky, 1987; Lino et al., 2018). Indeed, reminiscent of B-1a cells, 20% of adult CD138+TACI+IgM+ PCs were time-stamped by E17.5 and almost half by day 19 (Figures 1F, S1A, and S1D). More unexpectedly, we found that BM IgA PCs were similarly enriched for time-stamped cells (Figures 1F and S1A). This led us to look in the small intestinal lamina propria (SI-LP, Figure S1E), which is the largest site for anti-microbial IgA production in the body. We found that approximately half of SI-LP IgA PCs stem from B cells emerging within a narrow postnatal window between day 5 and day 10 (Figures 1G, 1H, and S1A). In day 19 time-stamped mice, essentially all Tom+ cells in the SI-LP consisted of IgA PCs (Figure S1F), which were evenly scattered across the LP as shown by immunofluorescence (Figure 1I). Thus, a portion of IgA PCs originates from B cells that share an overlapping developmental window with B-1a cells during unperturbed hematopoiesis. We conclude that the adult B cell pool harbors substantial contribution of cells predominantly emerging within the first 2 weeks of life (Figure 1J). These ELO-B cells overlap with IgM and IgA PCs known to produce natural and anti-microbial antibodies at steady state.

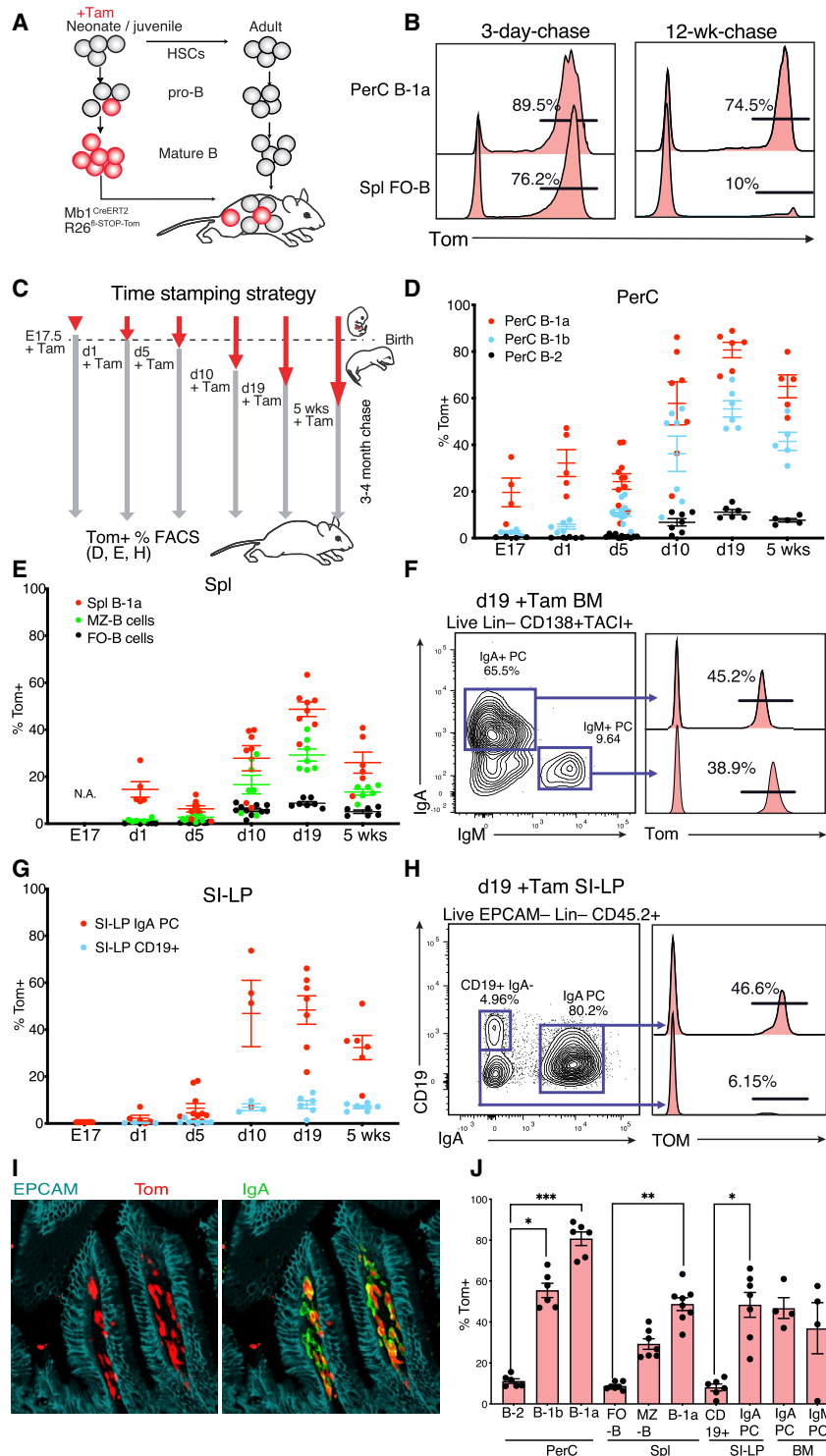


Figure 1. Time-stamping of early-life-origin B cells in adult mice

(A) B cell lineage-tracing model. A single dose of Tam administered at an early-life time point to Mb1^{CreERT2} R26^{fl-STOP-Tom} mice is designed to label developing and pre-existing B lineage cells at the time of treatment while leaving subsequent B cell output unlabeled.

(B) Representative histograms show Tom+ frequency in total peritoneal cavity (PerC) B-1a (Lin- CD19+ CD43+ CD23- CD5+) and splenic (Spl) FO-B (Lin- CD19+ CD93- CD23+) cells at 3 days and 12 weeks following day 19 Tam administration measured by FACS.

(C) Scheme depicting the serial time-stamping strategy for resolving the developmental window of early-life-derived B cells present in adult mice. Mice received a single dose of Tam at the indicated time points and were analyzed for Tom frequency by FACS following a 12–16-week chase period.

(D, E, and G) Tom labeling results from (C) for the indicated B cells subsets (n = 4–9) from the (D) PerC, (E) Spl, and (G) small intestinal lamina propria (SI-LP) (mean ± standard error of the mean [SEM]).

(F and H) Representative FACS analysis of Tom labeling frequency of day-19 time-stamped mice in (F) bone marrow (BM) IgA and IgM plasma cells (PCs) and (H) SI-LP IgA PCs and CD19+ cells at 12 weeks of chase. Gating strategies for (B)–(H) are shown in Figure S1A.

(I) Immunofluorescence of small intestinal villi identifying Tom+ IgA PCs residing in the SI-LP of day 19 time-stamped mice at 6 months of chase.

(J) Summary of Tom+ frequency in day 19 time-stamped mice reflecting the relative abundance of early-life-origin B (ELO-B) cells within the analyzed B cell subsets (n = 4–9, mean ± SEM). Statistics calculated using Kruskal-Wallis test (*p ≤ 0.05, **p ≤ 0.01, ***p ≤ 0.001).

CD5+ B-1a cells exhibited remarkable stability in labeling without any noticeable decline (Figure 2A). The CD5- B-1b cells in the PerC exhibited a 50% decline in Tom+ frequency within the 3–6 month chase period after which labeling was stable. These data are consistent with the ability of PerC B-1 subsets to self-sustain, whereas splenic B cells exhibit an overall higher replacement rate. The SI-LP IgA PCs displayed a slow decline in Tom frequency from 50% to 25% over the course of 18 months (Figure 2C). This relative stability in Tom labeling was also seen in the BM (Figure S2A) and is in line with longevity of gut IgA PCs in mice

Early-life-origin IgA PCs are actively maintained

To track the long-term erosion of Tom+ frequency with age, we analyzed day 19 time-stamped mice at various time points up to 18 months of chase (Figures 2A–2C and S2A). While Tom+ B cell subsets in the spleen declined to background levels within the 3–12 month chase period (Figure 2B), PerC

and humans (Hapfelmeier et al., 2010; Landsverk et al., 2017; Lemke et al., 2016). To address whether the abundance of time-stamped IgA PCs is a mere function of their longevity or whether such cells can be actively maintained from precursors, we induced their acute depletion by bortezomib (BZ) treatment (Lindner et al., 2012). Efficacy of the depletion

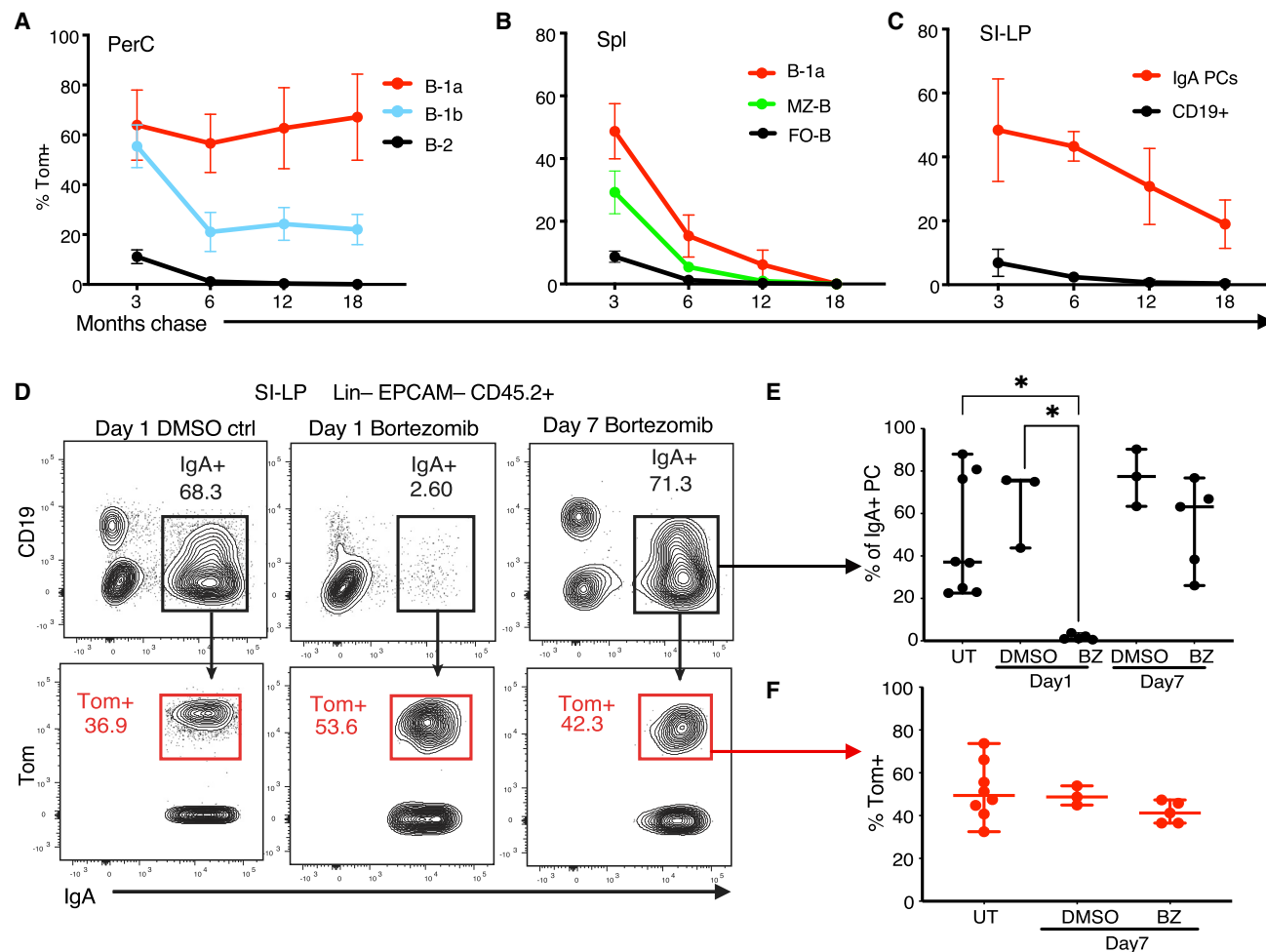


Figure 2. SI-LP IgA PCs are actively maintained by a reservoir of ELO-B cell precursors

(A–C) Day 19 time-stamped mice were analyzed for Tom+ frequency in the indicated B cell subsets of the (A) PerC, (B) Spl, and (C) SI-LP by FACS. $n = 3–8$ for each group from 3 independent experiments (mean \pm SEM).

(D–F) Day 19 time-stamped mice were BZ treated on two consecutive days at 12 weeks of chase (Lindner et al., 2012) (see STAR Methods for details). Data from 2 independent experiments.

(D) Representative FACS plots show frequencies of IgA PCs and their Tom+ frequency in the SI-LP at the indicated time points following the last BZ treatment. (E) Frequency of IgA+ PC in the SI-LP following BZ treatment (median \pm range). Statistics calculated using Kruskal-Wallis test (* $p \leq 0.05$, ** $p \leq 0.01$, *** $p \leq 0.001$). See Figure S2B for per experiment deconvoluted data.

(F) Tom+ frequency of the IgA PC compartment following BZ treatment (median \pm range).

regimen was near complete, and IgA PC recovery was observed 7 days later as previously reported (Figures 2D, 2E, and S2B). Remarkably, recalled SI-LP IgA PCs displayed near identical Tom+ frequency compared with DMSO-treated mice (Figure 2F). This result is in line with a previous study that reported the recovery of pre-existing IgA PC clones following BZ treatment (Lindner et al., 2012) and demonstrates that the IgA PC compartment is actively maintained by a reservoir of early-origin B cells.

Early-life-derived IgA clones are archived in multiple ELO-B cell compartments

The main inductive site for the generation of SI-LP IgA PCs are the Peyer’s patches (PPs), which harbor the so-called chronic GCs that sustain diversification of the IgA repertoire (Reboldi

and Cyster, 2016). In search of ELO-B cell precursors to IgA PCs, we analyzed PPs from day 19 time-stamped mice for Tom+ frequency. UMAP analysis of CD19+ PP B cells was performed on FACS data based on the surface expression of CD38, CD73, IgD, and CD19 (Tomayko et al., 2010) to reduce dimensionality (Figure 3A). This analysis showed that while the naive B cell compartment (IgD+CD38+CD73–) was largely devoid of Tom+ B cells (<5%), both the chronic GC B cell compartment (IgDlo/–CD38–CD73+GL7+) (16.5%) and the immunophenotypic MBC compartment (IgDlo/–CD38+CD73+) (19%) were enriched for Tom+ B cells (Figures 3A, 3B, and S3A). This finding is consistent with previous work demonstrating memory-like longevity in chronic GC B cells (Le Gallou et al., 2018). We conclude that ELO-B cells make up a sizeable fraction of antigen-experienced B cells in the PPs of unperturbed adult mice.

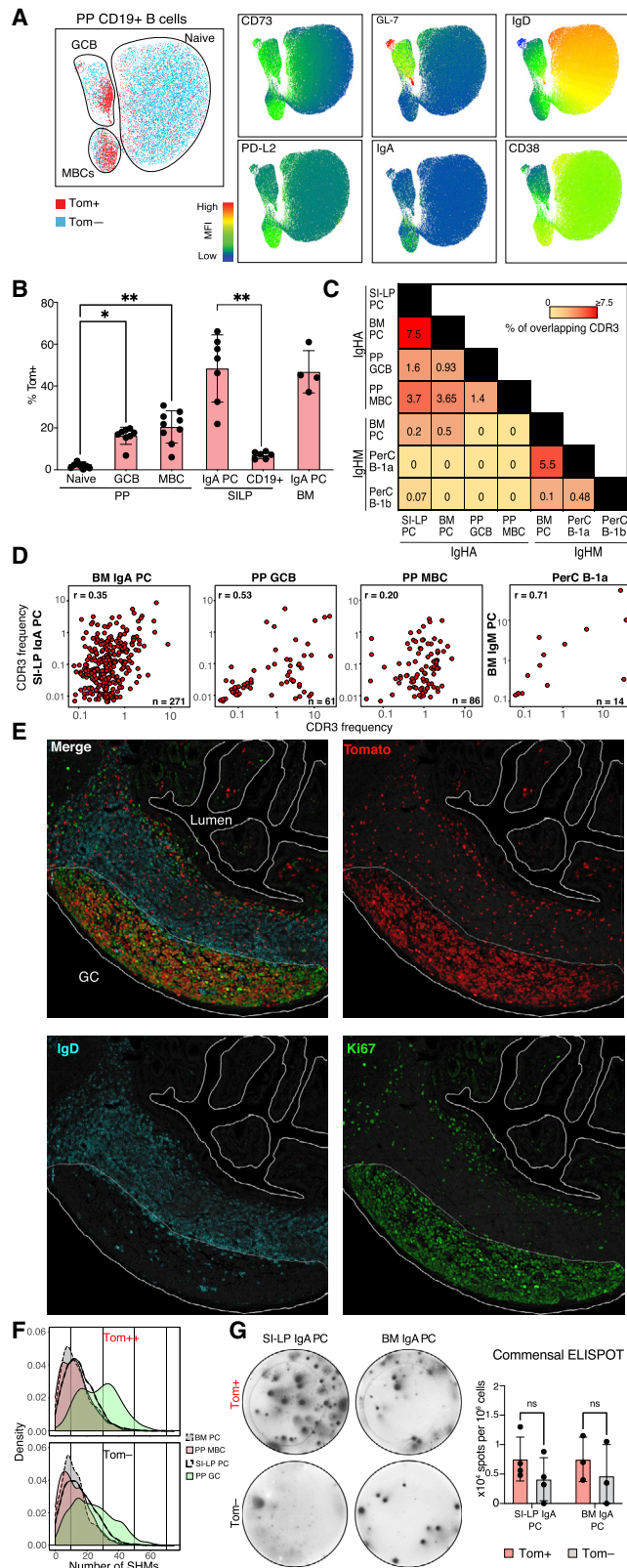


Figure 3. Early-life-derived IgA clones are archived in multiple mucosal and systemic B cell compartments

Data show analyses from day 19 time-stamped mice at 3–4 months of chase. (A) (Left) Representative UMAP visualization of FACS data of CD19+ B cells from Peyer’s patches (PPs). Fluorescence intensity parameters used for the UMAP generation were CD73, CD38, IgD, and CD19 and clearly resolve three major subsets. Tom+ B cell distribution across these is shown in red. (Right) Heatmaps show distribution of fluorescence intensity of the indicated markers. (B) Summary of Tom+ frequency within the indicated B cell subsets (n = 4–9, mean ± standard deviation [SD]). (C) Matrix shows frequency of overlapping CDR_{H3} amino acid identities among the indicated Tom+ B cell populations as determined by IgHA or IgHM VDJ-seq data analysis. Frequency was calculated as the number of overlapping CDR_{H3}s divided by the sum of the total number of unique CDR_{H3}s. Data are from 3 biological replicates except MBC (n = 2). Per mouse deconvoluted data are shown in Figure S3B. (D) Plots show frequency correlation of overlapping CDR_{H3}s for the indicated populations. (E) Immunofluorescence of a PP shows Tom+ B cells in the IgD–Ki67+ germinal center (GC). (F) Histograms show the distribution of somatic hypermutations (SHMs) among unique clones within Tom+ and Tom– IgA B cell subsets as determined by IgHA VDJ-seq analysis. Clones were defined by collapsing sequences sharing identical V_H, D_H, J_H segment usage, and CDR_{H3} nucleotide sequence. Data were obtained by collapsing unique clones from n = 3 biological replicates (except for MBC [n = 2]) and therefore not weighted by clone size and lack statistical significance. Per mouse deconvoluted data are shown in Figure S3D. (G) Detection of commensal reactive IgA PCs by ELISPOT. Left panel shows representative wells of the indicated populations. Bar plot summarizes the spot count normalized to 10⁶ cells of the Tom+ and Tom– subsets analyzed (n = 3–4 from two independent experiments, mean ± SD). Statistics were calculated using Kruskal-Wallis test (*p ≤ 0.05, **p ≤ 0.01, ***p ≤ 0.001).

We next performed IgHA and IgHM repertoire analysis to assess the clonal relatedness between ELO-B cell populations (Table S1; Data S1). CDR_{H3} clonal overlap and frequency correlation between various Tom+ subsets were calculated (Figures 3C, 3D, S3B, and S3C). Our results identified a notable fraction of shared CDR_{H3}s among the different IgA+ subsets (Figures 3C and S3B), suggesting that IgA+ ELO-B clones are archived in multiple gut-associated B cell compartments. Interestingly, although IgM+ ELO-B cell subsets shared considerable CDR_{H3}s with each other, virtually no overlap was detected with the IgA compartment. Hence, our results suggest that they do not frequently contribute to mucosal responses in unimmunized adult mice. CDR_{H3} frequency correlation of overlapping clones represents a sensitive measure of relatedness between two B cell compartments. We detected the highest CDR_{H3} frequency correlation between Tom+ SI-LP PCs and GC B cells, consistent with chronic GC B cells being a major source for ELO IgA SI-LP PC replenishment (Figure 3D). Taken together, we conclude that ELO PCs, MBCs, and chronic GC B cells form a layer of self-sustaining IgA memory in unimmunized adult mice that archive and maintain early-life-induced IgA production.

Early-life-derived IgA clones undergo continuous selection in chronic germinal centers

To visualize the distribution of ELO-B cells in the PP, we performed immunofluorescence microscopy (Figure 3E). We observed a remarkable concentration of time-stamped B cells within the chronic GC structures in line with our FACS data (Figures 3A and 3B). Recent studies have cemented the notion

that chronic GC B cells undergo continuous affinity maturation under homeostatic conditions (Chen et al., 2020; Nowosad et al., 2020). To this end, we detected a striking accumulation of somatic hypermutations (SHMs) among unique Tom+ GC B cell clones, which exceeded the levels in their Tom- counterparts (Figures 3F and S2D). Thus, our results strongly suggest that GC clones of ELO-B cell origin represent some of the most affinity-matured “winner clones” in PPs of unimmunized adult mice. Importantly, Tom+ GC B cells exhibit higher levels of SHMs compared with both PCs and MBCs (Figures 3F and S2D). This finding is consistent with the slow turnover of the latter two memory compartments at steady state (Bemark et al., 2016; Lemke et al., 2016). Indeed, Tom+ SI-LP IgA PCs from aged mice exhibited increased SHM accumulation (Figure S2E), suggesting that increasingly affinity-matured clones from the GC slowly replace long-lived IgA PCs. As expected, no significant accumulation of SHMs was detected among the IgM+ ELO-B cell subsets (Figure S3F). Taken together, these findings demonstrate the sustained active involvement of IgA+ ELO-B cells in clonal selection and affinity maturation within chronic GCs of the gut.

Commensal microbiota is the predominant driver of chronic IgA responses in the gut (Hapfelmeier et al., 2010). To assess the distribution of commensal reactivity among Tom+ and Tom- IgA PCs, we performed anti-commensal ELISPOT assays (Rojas et al., 2019) on sorted subsets. Adult commensal reactive IgA PCs were detected in both the Tom+ and Tom- fractions of the SI-LP as well as BM (Figure 3G). Interestingly, Tom+ IgA PCs exhibited a slight but not significant increase in the frequency of commensal reactivity. Together with our time-stamping results (Figure 1H), this finding shows that at least half of the commensal reactive IgA PCs under homeostatic conditions are of ELO-B cell origin. To investigate whether microbiota perturbation has any differential impact on ELO-B cell-driven IgA responses, we treated time-stamped adult mice with broad spectrum antibiotics in the drinking water for 4 weeks. FACS analyses showed a significant decrease in the Tom+ frequency of SI-LP and BM IgA PCs as well as a trend toward reduced Tom+ representation among chronic GC B cells of the PPs following treatment (Figure S3G). These results demonstrate that chronic ELO-B cell-driven IgA responses are dynamically controlled by microbial abundance. Taken together, we conclude that commensal microbiota is a key driver of ELO-B cell-derived IgA responses in unimmunized adult mice.

ELO-B cells harbor unique clones induced by early-life exposure

Developmental changes in the pre-immune B cell repertoire from neonatal to adult life is well documented (Perlmutter et al., 1985; Schroeder et al., 1987). Indeed, neonatal immunization with group A *Streptococcus* recruits unique clones into the long-lived memory pool not found in adult mice immunized by the same antigen (New et al., 2020). To qualitatively compare ELO-B cell-derived IgA memory with adult-derived IgA memory, we turned to an established model for gut infection. Oral RV infection elicits a robust mucosal IgA response that protects against reinfection (Franco and Greenberg, 1995) and therefore offers a more controlled and antigen-specific approach to interrogate the memory of early-life microbial exposure in the gut. Day 19 time-stamped mice were orally infected with the murine RV

strain EC_w either as adults or 5-day-old neonates (Figures 4A and 4B). The frequency of antigen-specific SI-LP IgA PCs was measured using GFP conjugated RV virus-like particles (VLPs) constructed from VP2 and the immunodominant VP6 (Figures 4A and 4B) (Nakawesi et al., 2021). In adult infected mice, VLP+ PCs at 2 and 9 weeks post infection were largely devoid of Tom+ cells (Figures 4A and 4C), suggesting that ELO-B cells are not major contributors to IgA memory formation in adult mice despite their relative abundance in the gut. In contrast, VLP+ IgA PCs generated from day 5 infection were as expected predominantly Tom+ 9 weeks later (Figures 4B and 4C). Similar patterns of Tom labeling were observed in the BM VLP+ IgA PC compartment (Figures 4D, S3A, and S3B). These results demonstrate that ELO-B cell-derived IgA PCs are imprinted by the memory of neonatal gut antigen exposure.

To investigate whether neonatal versus adult RV infection promotes the recruitment of unique B cell receptor (BCR) clones, we performed IgHA repertoire profiling on FACS sorted VLP+ SI-LP PCs from day 5 and adult infected mice at week 2 and 9 post infection (Figures 4E and 4F; Table S2; Data S1). GC B and MBC repertoires were not assessed due to a lack of long-term detectable VLP+ clones (Figures S4C and S4D). Repertoire analyses revealed a polyclonal response in both adult and neonatally infected mice with an age-dependent usage of the V_H13-2 gene segment that is statistically significant (Figures 4G and 4H). To identify recurrent RV reactive BCR specificities, we merged the VLP+ IgHA sequence reads from all samples and collapsed them into clonal families as defined by V and J segment usage, junction length, and Hamming distance (0.1, see STAR Methods). Among the top 50 clonal families, 13 were found in 3 or more individual RV-infected mice (Figure 4I). Interestingly, the sequencing reads of 4 of these recurrent clonal families (#3, #8, #9, and #13) derived almost exclusively from neonatally infected mice, whereas 3 other families (#5, #10, and #11) were made up of reads entirely from adult infected mice (Figures 4J and S4E). Such age-specific recruitment of clonal responses to the same antigen is consistent with a non-redundant role for neonatal-derived memory (New et al., 2020). The V_H13-2 gene segment encodes for clone family #3, which is recurrently produced in the neonatal response (6 out of 7 mice) and not detectable in the adult (0/10) (Figures 4H–4K). The dominant clone in this family is largely devoid of non-templated nucleotide additions, a hallmark of neonatal B lymphopoiesis (Figure S4F; Li et al., 1993). These findings are consistent with qualitative differences in the neonatal pre-immune BCR repertoire and highlight the neonatal period as a window of opportunity for the recruitment of unique clones into long-lived B cell memory (Vergani and Yuan, 2021).

New infection recruits adult hematopoiesis-derived B cells

Primary intestinal infections recruit B cell clones that are distinct from those dominant under homeostatic conditions (Lindner et al., 2015). To directly test whether RV infection recruits adult BM-derived B cells, we employed *Fgd5Cre*^{ERT2}-driven lineage tracing. Upon Cre induction, this model allows for labeling of adult hematopoietic stem cell (HSC) output and has previously been used to demonstrate that adult HSCs contribute negligibly to the PerC CD5+ B-1a compartment *in situ* (Säwen et al., 2018).

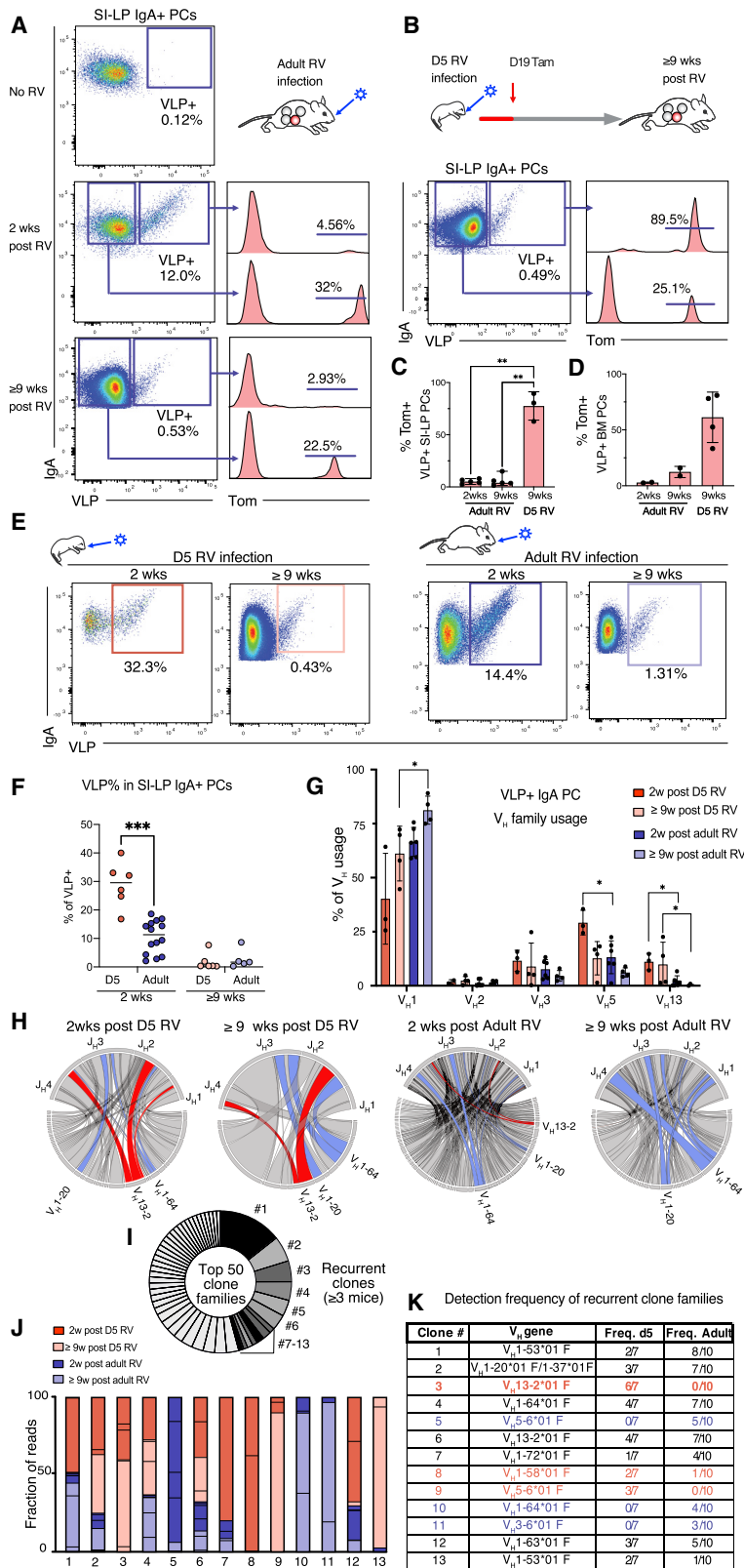


Figure 4. ELO-B cells carry unique memory induced by early-life rotavirus exposure

(A) Adult day 19 time-stamped mice were orally infected with rotavirus (RV) at 15 weeks of age. Representative FACS analyses at the indicated time points post infection show Tom+ frequency among antigen-specific (VLP+) and non-specific (VLP-) fractions of SI-LP IgA PCs. Mock infected No RV mouse lacks VLP+ IgA PCs.

(B) Neonates were infected on day 5, time-stamped by a single dose of Tam administration on day 19, and analyzed at 9 weeks post RV infection.

(C and D) Histograms show Tom+ frequency in VLP+ IgA PCs in the (C) SI-LP (n = 3–5, from 3 independent experiments) and (D) BM (n = 2–5, from 2 independent experiments) (mean ± SD). Statistics was calculated using Kruskal-Wallis test (*p ≤ 0.05, **p ≤ 0.01, ***p ≤ 0.001).

(E) Representative FACS analyses of VLP+ SI-LP IgA PCs from RV-infected day 5 and adult wild-type mice at 2 and 9 weeks post infection.

(F) Compiled summary of data shown in (E). Statistics using Kruskal-Wallis test (*p ≤ 0.05, **p ≤ 0.01, ***p ≤ 0.001).

(G–K) VLP+ SI-LP IgA PC immune repertoire analyses from sample groups in (E) as determined by IgHA V(D)J sequencing. n = 3 for 2 weeks and n = 4 for 9 weeks post infection of day 5 infected mice. n = 6 for 2 weeks and n = 4 for 9 weeks post infection of adult infected mice.

(G) Graph shows the 5 most commonly used V_H families among VLP+ IgA PCs. Read counts for each V_H family were pooled and calculated as a fraction of the total read counts (mean ± SD). Statistics using Mann-Whitney test (*p ≤ 0.05, **p ≤ 0.01, ***p ≤ 0.001).

(H) Circos plots depict B cell clones defined by V and J segment usage. Read counts were pooled from samples in each group. V_H13-2-containing clones are predominantly used by day 5 infected mice and marked in red. V_H1-20 and V_H1-64 containing clones represent examples of clones shared across all groups and are colored in blue.

(I) Pie-chart illustrates the top 50 VLP+ clone families identified from all samples combined (n = 16). Read number contribution from each biological sample was normalized. Clones are defined based on V and J usage, junction length, and Hamming distance of 0.1 (see STAR Methods for details). The 13 color-filled slices identify recurrent clone families shared between ≥ 3 mice.

(J) Bar graph illustrates sample contribution to each of the recurrent clone families.

(K) Table indicating the IGHV segment usage for the 13 recurrent clone families and their detection frequency in day 5 versus adult infected mice. Red text denotes clone families unique to neonatal infected mice, whereas blue text denotes clone families unique to adult infected mice.

We initiated Cre induction at 5 weeks of age with a continuous Tam-containing diet regimen (Säwen et al., 2018) to time-stamp B cells generated after the attenuation of ELO-B cell output (Figure 5A). 5–6 months later, the peripheral FO-B cell compartment had reached 30%–40% labeling in accordance with the slow BM-dependent input to the B cell compartment in steady-state adult mice (Figures 5B and 5C; Förster and Rajewsky, 1990; Säwen et al., 2018). Despite subsaturated labeling, we observed the anticipated reversed time-stamp pattern compared with the *Mb1Cre^{ERT2}* model, demonstrating little labeling in the SI-LP IgA PCs, PP GC B, and MBC compartments comparable with that observed in PerC B-1a cells (Figures 5B–5D). In contrast, labeled cells were efficiently recruited to these antigen-experienced B cell populations 2 weeks post RV infection (Figures 5E–5H). Similar observations were made in adult time-stamped mice in response to oral ovalbumin (OVA) immunization (Figures S5A–S5E). Thus, the main role for adult HSC-derived B cells is to enable adaptation of the steady-state intestinal IgA response to new immune challenges.

IgA PCs are developmentally related to fetal-derived B-1a cells

B-1a cells emerge from HSPCs displaying fetal-specific lineage potential (Kristiansen et al., 2016). Our time-stamping results traced B-1a and IgA PCs to the same early-life developmental window. To investigate whether IgA PCs originate from the same fetal-specific HSPCs, we performed single-cell lineage tracing using lentiviral cellular barcoding. Multipotent HSPCs from E14.5 wild-type FLs were transduced with the barcode library LV-GFP-lib and transplanted into lethally irradiated recipient mice as previously described (Figure 6A; Kristiansen et al., 2016). In a transplantation setting, distinct short and long-lived donor stem and progenitor cells give rise to sequential waves of hematopoietic output in the recipient. To allow for the re-equilibration of homeostasis following transplantation, analyses were performed after a 16–20-week time period (Figure 6A; Kristiansen et al., 2016). Barcodes were sequenced from GFP+-sorted PerC CD5+ B-1, SI-LP IgA+ PCs, Spl FO-B, and SI-LP CD19+ B cells. Our results showed that IgA PCs share a considerable barcode overlap with B-1a cells demonstrating common precursors among tagged fetal HSPCs (Figures 6A and S6A). Frequency correlation among shared barcodes represents the most sensitive measure of developmental relatedness between two populations. Interestingly, IgA PCs shared a better barcode frequency correlation with B-1a cells compared with splenic FO-B cells (Figure 6B). In contrast, barcodes from splenic FO-B cells correlated best with SI-LP CD19+ cells (Figure 6B). These results are representative of three biological replicates and demonstrate a shared developmental path between IgA PCs and B-1a cells in a transplantation context.

PerC B-1a cells can give rise to SI-LP IgA upon adoptive transfer (Bunker et al., 2015; Kroese et al., 1989). However, we observed no overlap between CDR_H3 sequences obtained from Tom+ PerC B-1a and SI-LP IgA+ cells in unperturbed mice (Figure 3D). It was clear from these data that Tom+ PerC B-1a cells and their related BM IgM+ PCs are dominated by V_H11 and V_H12-encoding PtC-reactive BCRs (Figures 6C, 6D, and S6B–S6D) that were not detected in the IgA repertoire (Fig-

ure S6D). Taken together, our findings support a model in which B-1a cells arise from the same HSPCs as IgA PC cells during ontogeny but do not substantially contribute to IgA PC maintenance in steady-state adult mice.

To interrogate whether Tom+ B cells of time-stamped mice are capable of differentiating into IgA PCs upon appropriate stimulation, we sorted and cultured them under IgA-switching conditions *ex vivo* (Kaminski and Stavnezer, 2006). Our results showed that both PerC and splenic Tom+ B cells undergo IgA class switch recombination and differentiate into antibody-secreting cells (Figures 6E–6H). Interestingly, PtC reactivity was selectively excluded from the IgA-switched B cell fraction in the PerC (Figure S6E), consistent with the observation that V_H11 and V_H12 are not represented in the IgA repertoire (Figure 6C). A layer of splenic IgM memory has previously been shown to be induced by mucosal responses in the gut (Le Gallou et al., 2018). In line with this, we also detected commensal reactivity among IgA-switched PCs from Tom+ splenic B cells (Figure S6F). In summary, we propose that B-1a and IgA repertoires found in adult mice housed under specific pathogen free (SPF) conditions largely diverged in an antigen-driven manner from a common primary B cell repertoire early in life (Figure S6G). Furthermore, some but not all specificities of IgM ELO-B cells may be recruited to participate in IgA responses when the appropriate challenge is met.

DISCUSSION

In this study, we used a time-stamping approach to dissect functional heterogeneity in the adult B cell compartment based on developmental timing. Our results showed a high degree of developmental heterogeneity in the unperturbed adult B cell pool with a substantial contribution by ELO-B cells arising during the first 2 weeks of life. The observed frequency of ELO-B cells likely represents an underestimation of their true abundance due to our subsaturated labeling strategy. Traditionally, B-1 cells are classified alongside FO and MZ B cells as a distinct subset of naive B cells defined based on immunophenotype and anatomical location (Allman and Pillai, 2008). This notion is fueled by their presence in germ-free animals and their primordial origin previously believed to be embryonic and fetal (Baumgarth, 2011; Yang et al., 2015). However, our results demonstrated a predominantly neonatal developmental window shared with other antigen-experienced MBC compartments, challenging the definition of B-1 cells as a naive B cell subset. Evidence for prior activation of B-1 cells by self-antigens and foreign antigens are in fact clear in the literature. First, the incorporation and peripheral expansion of B-1a clones depend on self-antigen-driven positive selection (Arnold et al., 1994; Ferry et al., 2006; Hayakawa et al., 1999; New et al., 2020). Second, both exposure to microbiota and deliberate immunization during a restricted neonatal window can recruit memory clones into the adult immunophenotypic B-1a cell population (New et al., 2020). Thus, it appears that B-1a cells are in every sense an antigen-experienced B cell subset shaped by early-life exposure. Indeed, the innate-like functional characteristics ascribed to B-1a cells including self-maintenance, tissue residence, clonal dominance, and rapid PC differentiation also typify MBC behavior. For these reasons, B-1a

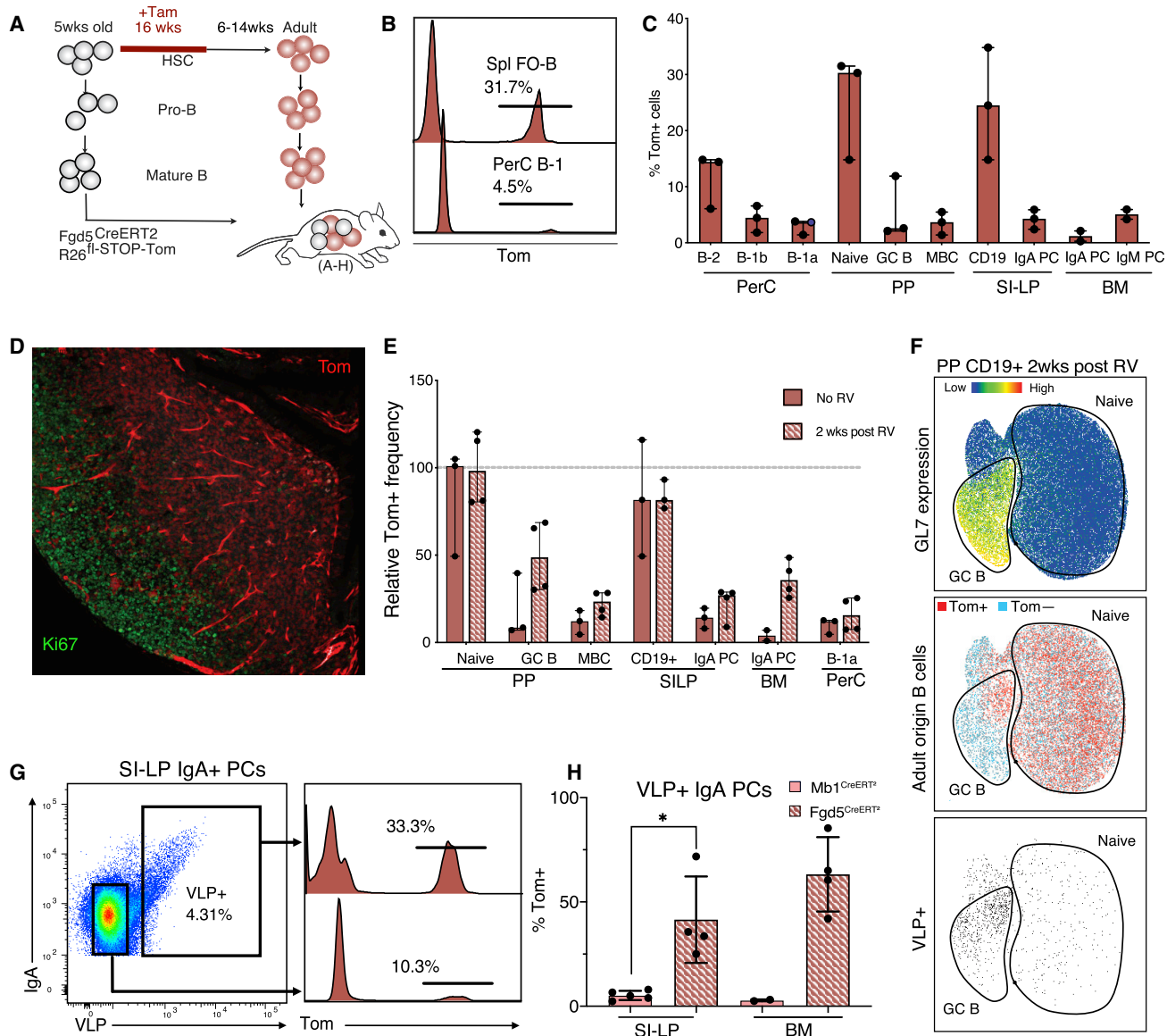


Figure 5. New infection recruits adult hematopoiesis-derived B cells

(A–F) Fgd5Cre^{ERT2} R26^{fl-STOP-Tom} mice were used to track the functional role of adult-derived B cells in the adult mouse at steady state and upon challenge. (A) Scheme of the Fgd5Cre^{ERT2} R26^{fl-STOP-Tom} model for tracing adult HSC output into the B cell compartment. Mice were kept on Tam-containing chow starting at 5 weeks of age for a 16-week labeling period and analyzed at 5–7 months after initial labeling. (B) Representative histograms show Tom+ frequency in the indicated populations. (C) Compiled frequencies of Tom+ cells within the indicated B cell subsets (n = 2–3, median ± range). (D) Immunofluorescence of a PP with anti-Ki67 staining (green) and Tom (red). (E) Compiled relative frequencies of Tom+ cells within the indicated B cell subsets in uninfected and RV-infected Fgd5Cre^{ERT2} time-stamped mice at 2 weeks post infection. Relative frequencies are normalized to mean of naive PP B cell labeling frequency. The observed differences are not statistically significant (n = 2–4, median ± range). (F) UMAP analysis of PP B cells from RV-infected mice at 2 weeks post infection. Top: GL-7 levels mark the GC cluster in UMAP generated using the following parameters (CD38, IgD, CD19). Middle: recruitment of adult-derived Tom+ B cells into the GC B fraction is evident. Bottom: VLP staining in the GC cluster overlaps with Tom+ B cells. (G) Representative FACS plots and histograms show Tom+ frequency in the VLP+ and VLP– SI-LP IgA+ PCs 2 weeks post RV infection. (H) Compiled summary of Tom+ frequencies in VLP+ IgA PCs from adult infected Mb1Cre^{ERT2} and Fgd5Cre^{ERT2} time-stamped mice (n = 5 for SI-LP, n = 2–4 for BM, mean ± SD). Statistics were calculated using Kruskal-Wallis test (significance is indicated as *p ≤ 0.05, **p ≤ 0.01, ***p ≤ 0.001).

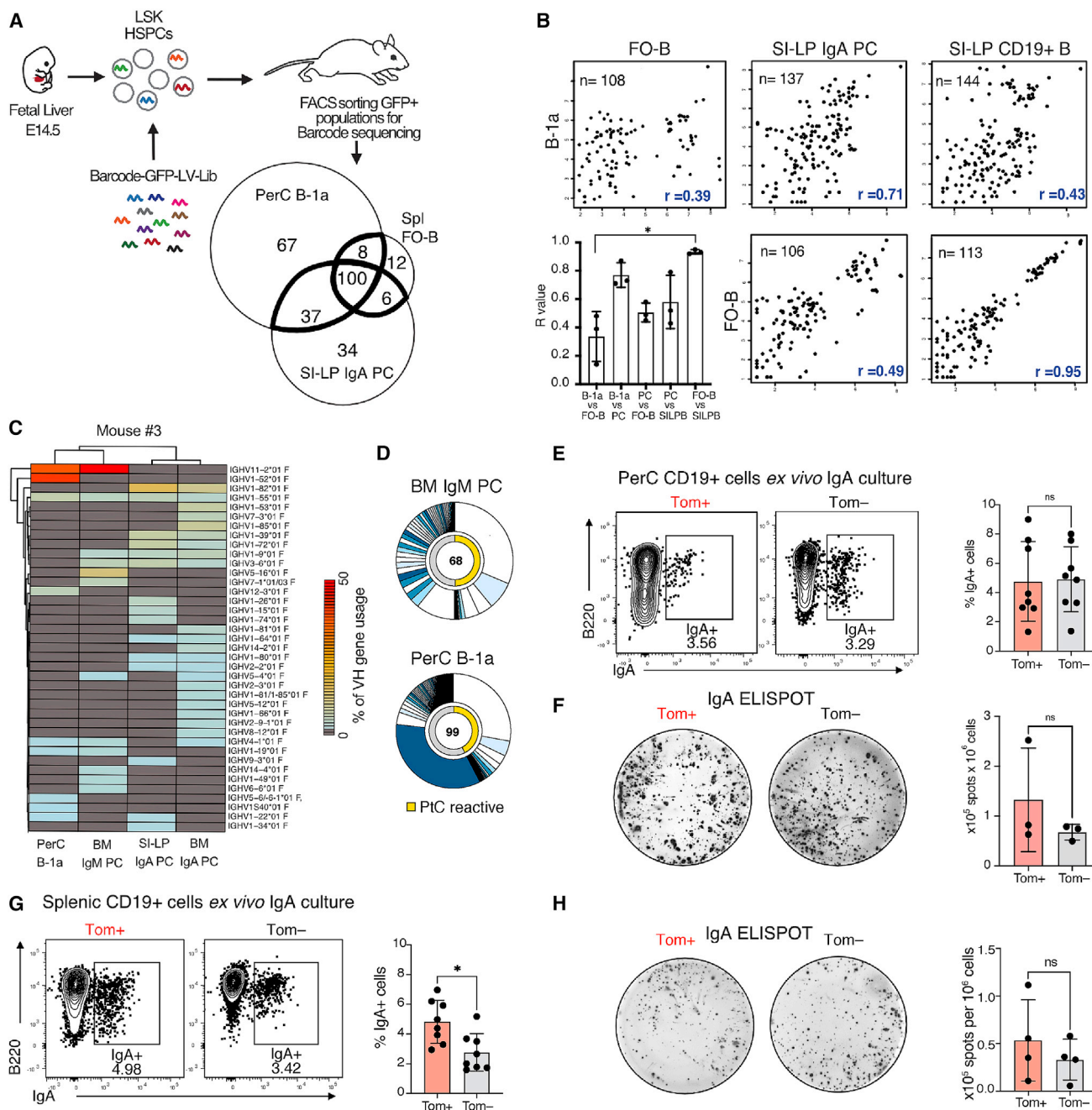


Figure 6. Interrogating the ontogenic relationship of B cell subsets

(A and B) Sorted fetal liver (FL) Lin⁺ Sca1⁺ cKit⁺ (LSK) HSPCs were transduced and transplanted into recipient mice as previously described (Kristiansen et al., 2016). After 16–20 weeks, the indicated donor-derived populations were FACS sorted for GFP positivity and used for downstream barcode sequencing. The results are representative of 3 biological replicates analyzed in two separate experiments.

(A) Venn diagrams show the number of overlapping and unique barcodes retrieved from the indicated populations. See Figure S6A for more details.

(B) Scatter plots show barcode read frequency correlations for the overlapping barcodes from the indicated populations. Bar plot summarises correlation indexes (mean \pm SD). Statistics were calculated using Kruskal-Wallis test (* $p \leq 0.05$, ** $p \leq 0.01$, *** $p \leq 0.001$).

(C) Heatmap illustrates V_H gene segment usage comparing the indicated B cell subsets. Representative of three biological replicates (see Figure S6B).

(D) Donut plots illustrate the clonal composition of the IgM repertoire of the indicated Tom+ B cell population from a representative mouse. Slices correspond to unique CDR_H3s and are sized proportionally to frequency. The total number of unique CDR_H3s identified is indicated in the middle. Yellow represents the fraction of V_H11 - and V_H12 -encoded PtC-reactive clones.

(E–H) Tom+ or Tom– CD19+ B cells from the indicated organs were sorted and individually cultured under IgA-switching conditions (LPS, TGF- β , and BAFF, see STAR Methods for details). 5 days post culture, the cells were subjected to FACS analysis (E and G) or IgA ELISPOT assays (F and H). Statistics were calculated using Kruskal-Wallis test (* $p \leq 0.05$, ** $p \leq 0.01$, *** $p \leq 0.001$).

(legend continued on next page)

cells can be more productively viewed as a predominantly neonatally induced IgM memory subset rather than a naive innate-like B cell. This updated classification offers a natural explanation to their poor contribution to GC reactions (Mesin et al., 2020) and memory formation. More importantly, it also demystifies their existence and phenotype in humans, which has remained a subject of debate (Tangye, 2013). In summary, our time-stamping results make clear that developmental timing and prior antigen experience are instrumental parameters in understanding the complexity of the adult peripheral B cell repertoire and calls for a revision of current textbook classification of B-1 cells as a “naive” B cell subset. By extension, we propose that similar thinking may be productive in the context of other semi-invariant lymphoid subsets (Bendelac et al., 2001) including MZ B cells, iNKT cells, and MAIT cells.

In addition to B-1 cells, we used two opposing time-stamping models to demonstrate that ELO-B cells harbor the memory of early-life gut exposure, making up a large proportion of antigen-experienced IgA B cell subsets in unimmunized adult mice. Adult origin B cells, on the other hand, predominated in the diverse naive BCR repertoire responsible for new antigen encounter. These findings resolve the division of labor between peripheral B cells of distinct ontogeny and highlight time-stamping as a powerful tool to study the long-term effects of neonatal immune imprinting. Our finding that early-life IgA memory was archived in various B cell compartments and actively maintained raised the question as to whether it is functionally distinct and therefore worthy of preservation. To this end, we used a model for RV infection to show that recurrent V_H13-2 encoded anti-RV clones are recruited upon neonatal infection but not detected in adult anti-RV responses. This finding mirrors a recent report demonstrating that neonatal immunization with group A streptococcus resulted in a unique clonal dominance profile of the antigen-specific B cell pool (New et al., 2020). Thus, similar to B-1 cells, IgA B cells of neonatal origin may serve a non-redundant role in the adult immune system. We conclude that antigen encounters during the neonatal window instruct distinct antigenic imprinting on memory formation with potential implications in vaccination strategies and the basis for the hygiene hypothesis (Bach, 2002).

Transfer of total PerC B cells into immunocompromised mice is able to reconstitute IgA PC cells in the gut of immune-compromised mice (Kroese et al., 1989). This along with evidence that IgA PCs can arise in CD40-deficient mice (Bergqvist et al., 2010) led to the notion that B-1 cells may be a major source of IgA PCs (Baumgarth, 2011). Indeed, our barcoding experiment revealed shared ancestors between PerC B-1a and gut IgA PCs at the HSPC level. However, VDJ-seq failed to detect any clonal overlap between these two subsets and instead indicate that chronic GC B cells and MBCs in the gut serve as the pre-

dominant memory reservoir responsible for IgA PC maintenance. Thus, although B-1a cells and IgA PCs share common progenitors during ontogeny, the former do not substantially contribute to the latter in unimmunized mice. We deduce from these complementary clonal-tracking readouts that the most likely bifurcation point between the two subsets is at the stage of antigen selection, where the nature of the antigen may dictate entry into either the IgM or the IgA arm of ELO-B cell memory. Indeed, this scenario is consistent with a classical view of memory formation and highlights the neonatal period as a key window for antigenic imprinting. Nevertheless, because B-1a cells do retain IgA-switching potential *in vitro*, we cannot rule out that appropriate activation signals may trigger B-1a to IgA conversion and gut homing *in vivo*.

Our observation that ELO-B cell contribution to various adult B cell compartments synchronously wanes after the first 2 weeks of life supports the notion of a strictly regulated developmental window. In addition to the onslaught of antigen exposure at birth and weaning, key molecular changes centered around the RNA-binding protein Lin28b also take place during this window to trigger a fetal to adult switch in hematopoietic output patterns (Kristiansen et al., 2018). Lin28b expression ceases by 2–3 weeks of age and is critical and sufficient to authorize the output of self-reactive B-1a cells early in life (Vanhee et al., 2019; Xu et al., 2020; Yuan et al., 2012). Considering the shared ontogeny between IgA PCs and B-1a cells, it is tempting to speculate whether the same molecular program also potentiates the output of ELO-B cells destined for mucosal IgA responses. Future studies aimed at determining the potential involvement of Lin28b and other molecular regulators in allowing for unique B cell memory formation open possibilities for the unprecedented exploitation and manipulation of the window of opportunity to improve immune intervention strategies.

In conclusion, these data unite a diverse category of developmentally related natural and microbiota-reactive B cells and unravel how the humoral arm of the adult adaptive immune system is hardwired by early postnatal exposure. Better understanding of the time restricted formation and non-redundant characteristics of ELO-B cells will generate valuable insights into the unique outcomes of early-life immunization and reveal the true impact of neonatal immune imprinting on life-long B cell immunity in health and disease.

Limitations of the study

It is important to acknowledge that although the observed enrichment for ELO-B cells among IgM and IgA memory compartments is true in adult mice housed under SPF conditions, we have not gathered any information on their abundance in the wild. Therefore, we cannot rule out that increased exposure to opportunistic infections and a more diverse microbiota may

(E) Left panel: representative FACS plots of indicated PerC IgA cultures. Right panel: bar plot summarizes the percentage of IgA⁺ cells from PerC IgA cultures (n = 8 from 3 independent experiments).

(F) Detection of IgA antibody-secreting cells (ASCs) by ELISPOT from PerC IgA cultures. Left panel: representative wells of the indicated populations. Right panel: bar plot summarizes the spot counts per 10^6 cells (n = 3 from two independent experiments, mean \pm SD).

(G) Left panel: representative FACS plots of indicated splenic IgA cultures. Right panel: bar plot summarizes the percentage of IgA⁺ cells from splenic IgA cultures (n = 8 from 3 independent experiments, mean \pm SD).

(H) Detection of IgA ASCs by ELISPOT from splenic IgA cultures. Left panel: representative wells of the indicated populations. Right panel: bar plot summarizes the spot counts per 10^6 cells (n = 4 from two independent experiments, mean \pm SD).

expand the representation of adult-derived B cell memory, thereby reducing the frequency of early-life-derived clones. However, it is equally possible that ELO-B cell memory induction might be more robust in the wild to generate a broader spectrum of clones that continue to evolve with life-long changes in the composition of commensal microbiota. Future co-housing experiments of time-stamped SPF mice with “dirtier” feral mice will be an important first step to addressing the influence of increased microbial pressure on the developmental composition of adult gut-associated B cell subsets.

Another important outstanding question is whether unique qualitative characteristics such as epitope affinity and poly-reactivity exist to make neonatal specific clones functionally distinct from, or more beneficial than, adult-derived clones. Indeed, the neonatal pre-immune B cell repertoire favors germ-line encoded and self/poly-reactive specificities that may influence adaptability to future cognate antigen encounters as well as cross-reactivity to unrelated self-antigens or non-self-antigens (Kearney et al., 2015). Furthermore, self-reactivity may also augment tonic signaling levels and the long-term fitness of a memory clone. Future studies elucidating the unique qualities of early-life-derived clones will reveal the basis for neonatal exposure as a unique “window of opportunity” to imprint long-term B cell memory.

STAR★METHODS

Detailed methods are provided in the online version of this paper and include the following:

- KEY RESOURCES TABLE
- RESOURCE AVAILABILITY
 - Lead contact
 - Materials availability
 - Data and code availability
- EXPERIMENTAL MODEL AND SUBJECT DETAILS
 - Animals
- METHOD DETAILS
 - Tamoxifen induction
 - Bortezomib treatment
 - Antibiotics treatment
 - Oral immunization with ovalbumin
 - Organ harvesting and flow cytometry
 - Immunofluorescence staining and confocal microscopy
 - Lentiviral barcoding
 - VDJ sequencing and analysis
 - Cell cultures
 - ELISPOT assays
 - Rotavirus stock preparation
 - Rotavirus infection
- QUANTIFICATION AND STATISTICAL ANALYSIS
 - Statistical analysis

SUPPLEMENTAL INFORMATION

Supplemental information can be found online at <https://doi.org/10.1016/j.immuni.2022.08.018>.

ACKNOWLEDGMENTS

We thank Dr. J.A. Daniel for his critical input and Karin Olsson for her technical support. We thank Dr. Marie Jönsson for graphical support. We acknowledge Protein Production Sweden (PPS) for providing facilities and experimental support, and we would like to thank Wolfgang Knecht and Celeste Sele for assistance. PPS is funded by the Swedish Research Council as a national research infrastructure.

Funding: J.Y. was supported by the European Research Council (715313), Knut and Alice Wallenberg Foundation (2019-0310), and the Swedish Research Council (2018-02712). K.L. was supported by the Swedish Research Council (2020-01977), the Ragnar Söderberg Foundation Fellowship, the Lundbeck Foundation Fellowship, the Crafoord Foundation, the Celiac Foundation, and the Gyllenstiernska Krapperup Foundation.

AUTHOR CONTRIBUTIONS

J.Y. and S. Vergani designed the study. S. Vergani performed all the experiments and analyses with the support of A.D. K.G.M. and J.N. contributed to the RV infection experiments, and K.L. provided the RV infection model, reagents, and ethical permit. A.D., T.A.K., and K.K. contributed to the barcoding experiments. C.D.S. performed the immunofluorescence experiments. G.M., N.K., S. Vanhee, and H.Å. contributed to the VDJ-seq and analysis. S.L.G. contributed to OVA immunization experiments and S.S. contributed to the commensal ELISPOT experiments. D.B. provided *FGD5Cre^{ERT2}* mice and expertise. K.L., W.W.A., and D.B. provided critical expertise and feedback. J.Y. conceived and supervised the study and wrote the paper together with S. Vergani.

DECLARATION OF INTERESTS

The authors declare no competing interests.

Received: September 8, 2021

Revised: May 20, 2022

Accepted: August 24, 2022

Published: September 16, 2022

REFERENCES

- Al Nabhani, Z., Dulauroy, S., Marques, R., Cousu, C., Al Bounny, S., Déjardin, F., Sparwasser, T., Bérard, M., Cerf-Bensussan, N., and Eberl, G. (2019). A weaning reaction to microbiota is required for resistance to immunopathologies in the adult. *Immunity* 50, 1276–1288.e5. <https://doi.org/10.1016/j.immuni.2019.02.014>.
- Allman, D., and Pillai, S. (2008). Peripheral B cell subsets. *Curr. Opin. Immunol.* 20, 149–157. <https://doi.org/10.1016/j.coi.2008.03.014>.
- Arnold, L.W., Pennell, C.A., McCray, S.K., and Clarke, S.H. (1994). Development of B-1 cells: segregation of phosphatidyl choline-specific B cells to the B-1 population occurs after immunoglobulin gene expression. *J. Exp. Med.* 179, 1585–1595. <https://doi.org/10.1084/jem.179.5.1585>.
- Bach, J.F. (2002). The effect of infections on susceptibility to autoimmune and allergic diseases. *N. Engl. J. Med.* 347, 911–920. <https://doi.org/10.1056/NEJMra020100>.
- Baumgarth, N. (2011). The double life of a B-1 cell: self-reactivity selects for protective effector functions. *Nat. Rev. Immunol.* 11, 34–46. <https://doi.org/10.1038/nri2901>.
- Bemark, M., Hazanov, H., Strömberg, A., Komban, R., Holmqvist, J., Köster, S., Mattsson, J., Sikora, P., Mehr, R., and Lycke, N.Y. (2016). Limited clonal relatedness between gut IgA plasma cells and memory B cells after oral immunization. *Nat. Commun.* 7, 12698. <https://doi.org/10.1038/ncomms12698>.
- Bendelac, A., Bonneville, M., and Kearney, J.F. (2001). Autoreactivity by design: innate B and T lymphocytes. *Nat. Rev. Immunol.* 1, 177–186. <https://doi.org/10.1038/35105052>.
- Bergqvist, P., Stensson, A., Lycke, N.Y., and Bemark, M. (2010). T cell-independent IgA class switch recombination is restricted to the GALT and occurs

- prior to manifest germinal center formation. *J. Immunol.* 184, 3545–3553. <https://doi.org/10.4049/jimmunol.0901895>.
- Bunker, J.J., Flynn, T.M., Koval, J.C., Shaw, D.G., Meisel, M., McDonald, B.D., Ishizuka, I.E., Dent, A.L., Wilson, P.C., Jabri, B., et al. (2015). Innate and adaptive humoral responses coat distinct commensal bacteria with immunoglobulin A. *Immunity* 43, 541–553. <https://doi.org/10.1016/j.immuni.2015.08.007>.
- Burns, J.W., Krishnaney, A.A., Vo, P.T., Rouse, R.V., Anderson, L.J., and Greenberg, H.B. (1995). Analyses of homologous rotavirus infection in the mouse model. *Virology* 207, 143–153.
- Busch, K., and Rodewald, H.R. (2016). Unperturbed vs. post-transplantation hematopoiesis: both in vivo but different. *Curr. Opin. Hematol.* 23, 295–303. <https://doi.org/10.1097/MOH.0000000000000250>.
- Charpilienne, A., Nejmeddine, M., Berois, M., Parez, N., Neumann, E., Hewat, E., Trugnan, G., and Cohen, J. (2001). Individual rotavirus-like particles containing 120 molecules of fluorescent protein are visible in living cells. *J Biol Chem* 276, 29361–29367. <https://doi.org/10.1074/jbc.M101935200>.
- Chen, H., Zhang, Y., Ye, A.Y., Du, Z., Xu, M., Lee, C.S., Hwang, J.K., Kyritsis, N., Ba, Z., Neuberger, D., et al. (2020). BCR selection and affinity maturation in Peyer's patch germinal centres. *Nature* 582, 421–425. <https://doi.org/10.1038/s41586-020-2262-4>.
- Constantinides, M.G., Link, V.M., Tamoutounour, S., Wong, A.C., Perez-Chaparro, P.J., Han, S.J., Chen, Y.E., Li, K., Farhat, S., Weckel, A., et al. (2019). MAIT cells are imprinted by the microbiota in early life and promote tissue repair. *Science* 366. <https://doi.org/10.1126/science.aax6624>.
- Ferry, H., Crockford, T.L., Leung, J.C., and Cornall, R.J. (2006). Signals from a self-antigen induce positive selection in early B cell ontogeny but are tolerogenic in adults. *J. Immunol.* 176, 7402–7411. <https://doi.org/10.4049/jimmunol.176.12.7402>.
- Förster, I., and Rajewsky, K. (1987). Expansion and functional activity of Ly-1+ B cells upon transfer of peritoneal cells into allotype-congenic, newborn mice. *Eur. J. Immunol.* 17, 521–528. <https://doi.org/10.1002/eji.1830170414>.
- Förster, I., and Rajewsky, K. (1990). The bulk of the peripheral B-cell pool in mice is stable and not rapidly renewed from the bone marrow. *Proc. Natl. Acad. Sci. USA* 87, 4781–4784. <https://doi.org/10.1073/pnas.87.12.4781>.
- Franco, M.A., and Greenberg, H.B. (1995). Role of B cells and cytotoxic T lymphocytes in clearance of and immunity to rotavirus infection in mice. *J. Virol.* 69, 7800–7806. <https://doi.org/10.1128/JVI.69.12.7800-7806.1995>.
- Gazit, R., Mandal, P.K., Ebina, W., Ben-Zvi, A., Nombela-Arrieta, C., Silberstein, L.E., and Rossi, D.J. (2014). Fgd5 identifies hematopoietic stem cells in the murine bone marrow. *J. Exp. Med.* 211, 1315–1331. <https://doi.org/10.1084/jem.20130428>.
- Ghosn, E., Yoshimoto, M., Nakauchi, H., Weissman, I.L., and Herzenberg, L.A. (2019). Hematopoietic stem cell-independent hematopoiesis and the origins of innate-like B lymphocytes. *Development* 146, dev170571. <https://doi.org/10.1242/dev.170571>.
- Ginhoux, F., and Williams, M. (2016). Tissue-resident macrophage ontogeny and homeostasis. *Immunity* 44, 439–449. <https://doi.org/10.1016/j.immuni.2016.02.024>.
- Gupta, N.T., Vander Heiden, J.A., Uduman, M., Gadala-Maria, D., Yaari, G., and Kleinstein, S.H. (2015). Change-O: a toolkit for analyzing large-scale B cell immunoglobulin repertoire sequencing data. *Bioinformatics* 31, 3356–3358. <https://doi.org/10.1093/bioinformatics/btv359>.
- Haas, K.M., Poe, J.C., Steeber, D.A., and Tedder, T.F. (2005). B-1a and B-1b cells exhibit distinct developmental requirements and have unique functional roles in innate and adaptive immunity to *S. pneumoniae*. *Immunity* 23, 7–18. <https://doi.org/10.1016/j.immuni.2005.04.011>.
- Hao, Z., and Rajewsky, K. (2001). Homeostasis of peripheral B cells in the absence of B cell influx from the bone marrow. *J. Exp. Med.* 194, 1151–1164. <https://doi.org/10.1084/jem.194.8.1151>.
- Hapfelmeier, S., Lawson, M.A., Slack, E., Kirundi, J.K., Stoel, M., Heikenwalder, M., Cahenzli, J., Velykoredko, Y., Balmer, M.L., Endt, K., et al. (2010). Reversible microbial colonization of germ-free mice reveals the dynamics of IgA immune responses. *Science* 328, 1705–1709. <https://doi.org/10.1126/science.1188454>.
- Hayakawa, K., Asano, M., Shinton, S.A., Gui, M., Allman, D., Stewart, C.L., Silver, J., and Hardy, R.R. (1999). Positive selection of natural autoreactive B cells. *Science* 285, 113–116. <https://doi.org/10.1126/science.285.5424.113>.
- Herzenberg, L.A., and Herzenberg, L.A. (1989). Toward a layered immune system. *Cell* 59, 953–954. [https://doi.org/10.1016/0092-8674\(89\)90748-4](https://doi.org/10.1016/0092-8674(89)90748-4).
- Hobeika, E., Levit-Zerdoun, E., Anastasopoulou, V., Pohlmeier, R., Altmeier, S., Alsadeq, A., Dobenecker, M.W., Pelanda, R., and Reth, M. (2015). CD19 and BAFF-R can signal to promote B-cell survival in the absence of Syk. *EMBO J.* 34, 925–939. <https://doi.org/10.15252/emboj.201489732>.
- Hornef, M.W., and Torow, N. (2020). 'Layered immunity' and the 'neonatal window of opportunity' - timed succession of non-redundant phases to establish mucosal host-microbial homeostasis after birth. *Immunology* 159, 15–25. <https://doi.org/10.1111/imm.13149>.
- Johansson-Lindbom, B., Svensson, M., Pabst, O., Palmqvist, C., Marquez, G., Förster, R., and Agace, W.W. (2005). Functional specialization of gut CD103+ dendritic cells in the regulation of tissue-selective T cell homing. *J. Exp. Med.* 202, 1063–1073. <https://doi.org/10.1084/jem.20051100>.
- Kaminski, D.A., and Stavnezer, J. (2006). Enhanced IgA class switching in marginal zone and B1 B cells relative to follicular/B2 B cells. *J. Immunol.* 177, 6025–6029. <https://doi.org/10.4049/jimmunol.177.9.6025>.
- Kantor, A.B., Stall, A.M., Adams, S., Watanabe, K., and Herzenberg, L.A. (1995). De novo development and self-replenishment of B cells. *Int. Immunol.* 7, 55–68. <https://doi.org/10.1093/intimm/7.1.55>.
- Kearney, J.F., Patel, P., Stefanov, E.K., and King, R.G. (2015). Natural antibody repertoires: development and functional role in inhibiting allergic airway disease. *Annu. Rev. Immunol.* 33, 475–504. <https://doi.org/10.1146/annurev-immunol-032713-120140>.
- Kristiansen, T.A., Doyle, A., and Yuan, J. (2017). Lentiviral barcode labeling and transplantation of fetal liver hematopoietic stem and progenitor cells. *Bio Protoc.* 7, e2242. <https://doi.org/10.21769/BioProtoc.2242>.
- Kristiansen, T.A., Jaensson Gyllenbäck, E., Zriwil, A., Björklund, T., Daniel, J.A., Sitnicka, E., Soneji, S., Bryder, D., and Yuan, J. (2016). Cellular barcoding links B-1a B cell potential to a fetal hematopoietic stem cell state at the single-cell level. *Immunity* 45, 346–357. <https://doi.org/10.1016/j.immuni.2016.07.014>.
- Kristiansen, T.A., Vanhee, S., and Yuan, J. (2018). The influence of developmental timing on B cell diversity. *Curr. Opin. Immunol.* 51, 7–13. <https://doi.org/10.1016/j.coi.2017.12.005>.
- Kroese, F.G., Butcher, E.C., Stall, A.M., Lalor, P.A., Adams, S., and Herzenberg, L.A. (1989). Many of the IgA producing plasma cells in murine gut are derived from self-replenishing precursors in the peritoneal cavity. *Int. Immunol.* 1, 75–84. <https://doi.org/10.1093/intimm/1.1.75>.
- Landsverk, O.J., Snir, O., Casado, R.B., Richter, L., Mold, J.E., Réu, P., Horneland, R., Paulsen, V., Yaqub, S., Aandahl, E.M., et al. (2017). Antibody-secreting plasma cells persist for decades in human intestine. *J. Exp. Med.* 214, 309–317. <https://doi.org/10.1084/jem.20161590>.
- Le Gallou, S., Zhou, Z., Thai, L.H., Fritzen, R., de Los Aires, A.V., Mègret, J., Yu, P., Kitamura, D., Bille, E., Tros, F., et al. (2018). A splenic IgM memory subset with antibacterial specificities is sustained from persistent mucosal responses. *J. Exp. Med.* 215, 2035–2053. <https://doi.org/10.1084/jem.20180977>.
- Lemke, A., Kraft, M., Roth, K., Riedel, R., Lammerding, D., and Hauser, A.E. (2016). Long-lived plasma cells are generated in mucosal immune responses and contribute to the bone marrow plasma cell pool in mice. *Mucosal Immunol.* 9, 83–97. <https://doi.org/10.1038/mi.2015.38>.
- Li, Y.S., Hayakawa, K., and Hardy, R.R. (1993). The regulated expression of B lineage associated genes during B cell differentiation in bone marrow and fetal liver. *J. Exp. Med.* 178, 951–960. <https://doi.org/10.1084/jem.178.3.951>.
- Li, Y.S., Wasserman, R., Hayakawa, K., and Hardy, R.R. (1996). Identification of the earliest B lineage stage in mouse bone marrow. *Immunity* 5, 527–535. [https://doi.org/10.1016/s1074-7613\(00\)80268-x](https://doi.org/10.1016/s1074-7613(00)80268-x).
- Lindner, C., Thomsen, I., Wahl, B., Ugur, M., Sethi, M.K., Friedrichsen, M., Smoczek, A., Ott, S., Baumann, U., Suerbaum, S., et al. (2015). Diversification of memory B cells drives the continuous adaptation of secretory

- antibodies to gut microbiota. *Nat. Immunol.* **16**, 880–888. <https://doi.org/10.1038/ni.3213>.
- Lindner, C., Wahl, B., Föhse, L., Suerbaum, S., Macpherson, A.J., Prinz, I., and Pabst, O. (2012). Age, microbiota, and T cells shape diverse individual IgA repertoires in the intestine. *J. Exp. Med.* **209**, 365–377. <https://doi.org/10.1084/jem.20111980>.
- Lino, A.C., Dang, V.D., L., V., Welle, A., Joedicke, J., Pohar, J., Simon, Q., Thalmensi, J., Baures, A., Fluhler, V., et al. (2018). LAG-3 inhibitory receptor expression identifies immunosuppressive natural regulatory plasma cells. *Immunity* **49**, 120–133.e9. <https://doi.org/10.1016/j.immuni.2018.06.007>.
- Lu, R., Neff, N.F., Quake, S.R., and Weissman, I.L. (2011). Tracking single hematopoietic stem cells in vivo using high-throughput sequencing in conjunction with viral genetic barcoding. *Nat. Biotechnol.* **29**, 928–933. <https://doi.org/10.1038/nbt.1977>.
- Madisen, L., Zwingman, T.A., Sunkin, S.M., Oh, S.W., Zariwala, H.A., Gu, H., Ng, L.L., Palmiter, R.D., Hawrylycz, M.J., Jones, A.R., et al. (2010). A robust and high-throughput Cre reporting and characterization system for the whole mouse brain. *Nat. Neurosci.* **13**, 133–140. <https://doi.org/10.1038/nn.2467>.
- Martin, F., Oliver, A.M., and Kearney, J.F. (2001). Marginal zone and B1 B cells unite in the early response against T-independent blood-borne particulate antigens. *Immunity* **14**, 617–629. [https://doi.org/10.1016/s1074-7613\(01\)00129-7](https://doi.org/10.1016/s1074-7613(01)00129-7).
- Melum, E., Jiang, X., Baker, K.D., Macedo, M.F., Fritsch, J., Dowds, C.M., Wang, J., Pharo, A., Kaser, A., Tan, C., et al. (2019). Control of CD1d-restricted antigen presentation and inflammation by sphingomyelin. *Nat. Immunol.* **20**, 1644–1655. <https://doi.org/10.1038/s41590-019-0504-0>.
- Mesin, L., Schiepers, A., Ersching, J., Barbulescu, A., Cavazzoni, C.B., Angelini, A., Okada, T., Kurosaki, T., and Victora, G.D. (2020). Restricted clonality and limited germinal center reentry characterize memory B cell reactivation by boosting. *Cell* **180**, 92–106.e11. <https://doi.org/10.1016/j.cell.2019.11.032>.
- Nakawesi, J., This, S., Hütter, J., Boucard-Jourdin, M., Barateau, V., Muleta, K.G., Gooday, L.J., Thomsen, K.F., López, A.G., Ulmert, I., et al. (2021). α -phavbeta8 integrin-expression by BATF3-dependent dendritic cells facilitates early IgA responses to Rotavirus. *Mucosal Immunol.* **14**, 53–67. <https://doi.org/10.1038/s41385-020-0276-8>.
- New, J.S., Dizon, B.L.P., Fucile, C.F., Rosenberg, A.F., Kearney, J.F., and King, R.G. (2020). Neonatal exposure to commensal-bacteria-derived antigens directs polysaccharide-specific B-1 B cell repertoire development. *Immunity* **53**, 172–186.e6. <https://doi.org/10.1016/j.immuni.2020.06.006>.
- Nowosad, C.R., Mesin, L., Castro, T.B.R., Wichmann, C., Donaldson, G.P., Araki, T., Schiepers, A., Lockhart, A.A.K., Bilate, A.M., Mucida, D., and Victora, G.D. (2020). Tunable dynamics of B cell selection in gut germinal centres. *Nature* **588**, 321–326. <https://doi.org/10.1038/s41586-020-2865-9>.
- Perlmutter, R.M., Kearney, J.F., Chang, S.P., and Hood, L.E. (1985). Developmentally controlled expression of immunoglobulin VH genes. *Science* **227**, 1597–1601. <https://doi.org/10.1126/science.3975629>.
- Reboldi, A., and Cyster, J.G. (2016). Peyer’s patches: organizing B-cell responses at the intestinal frontier. *Immunol. Rev.* **271**, 230–245. <https://doi.org/10.1111/imr.12400>.
- Rojas, O.L., Pröbstel, A.K., Porfilio, E.A., Wang, A.A., Charabati, M., Sun, T., Lee, D.S.W., Galicia, G., Ramaglia, V., Ward, L.A., et al. (2019). Recirculating intestinal IgA-producing cells regulate neuroinflammation via IL-10. *Cell* **176**, 610–624.e18. <https://doi.org/10.1016/j.cell.2018.11.035>.
- Sakaguchi, N., Kashiwamura, S., Kimoto, M., Thalmann, P., and Melchers, F. (1988). B lymphocyte lineage-restricted expression of mb-1, a gene with CD3-like structural properties. *EMBO J.* **7**, 3457–3464.
- Säwen, P., Eldeeb, M., Erlandsson, E., Kristiansen, T.A., Laterza, C., Kokaia, Z., Karlsson, G., Yuan, J., Soneji, S., Mandal, P.K., et al. (2018). Murine HSCs contribute actively to native hematopoiesis but with reduced differentiation capacity upon aging. *eLife* **7**, e41258. <https://doi.org/10.7554/eLife.41258>.
- Schroeder, H.W., Jr., Hillson, J.L., and Perlmutter, R.M. (1987). Early restriction of the human antibody repertoire. *Science* **238**, 791–793. <https://doi.org/10.1126/science.3118465>.
- Shi, W., Liao, Y., Willis, S.N., Taubenheim, N., Inouye, M., Tarlinton, D.M., Smyth, G.K., Hodgkin, P.D., Nutt, S.L., and Corcoran, L.M. (2015). Transcriptional profiling of mouse B cell terminal differentiation defines a signature for antibody-secreting plasma cells. *Nat. Immunol.* **16**, 663–673. <https://doi.org/10.1038/ni.3154>.
- Smith, N.L., Patel, R.K., Reynaldi, A., Grenier, J.K., Wang, J., Watson, N.B., Nzingha, K., Yee Mon, K.J., Peng, S.A., Grimson, A., et al. (2018). Developmental origin governs CD8(+) T cell fate decisions during infection. *Cell* **174**, 117–130.e4. <https://doi.org/10.1016/j.cell.2018.05.029>.
- Tangye, S.G. (2013). To B1 or not to B1: that really is still the question! *Blood* **121**, 5109–5110. <https://doi.org/10.1182/blood-2013-05-500074>.
- Tomayko, M.M., Steinel, N.C., Anderson, S.M., and Shlomchik, M.J. (2010). Cutting edge: hierarchy of maturity of murine memory B cell subsets. *J. Immunol.* **185**, 7146–7150. <https://doi.org/10.4049/jimmunol.1002163>.
- Vanhee, S., Åkerstrand, H., Kristiansen, T.A., Datta, S., Montano, G., Vergani, S., Lang, S., Ungerback, J., Doyle, A., Olsson, K., et al. (2019). Lin28b controls a neonatal to adult switch in B cell positive selection. *Sci. Immunol.* **4**, eaax4453. <https://doi.org/10.1126/sciimmunol.aax4453>.
- Vergani, S., and Yuan, J. (2021). Developmental changes in the rules for B cell selection. *Immunol. Rev.* **300**, 194–202. <https://doi.org/10.1111/imr.12949>.
- Xu, X., Deobagkar-Lele, M., Bull, K.R., Crockford, T.L., Mead, A.J., Cribbs, A.P., Sims, D., Anzilotti, C., and Cornall, R.J. (2020). An ontogenetic switch drives the positive and negative selection of B cells. *Proc. Natl. Acad. Sci. USA* **117**, 3718–3727. <https://doi.org/10.1073/pnas.1915247117>.
- Yang, Y., Wang, C., Yang, Q., Kantor, A.B., Chu, H., Ghosn, E.E., Qin, G., Mazmanian, S.K., Han, J., and Herzenberg, L.A. (2015). Distinct mechanisms define murine B cell lineage immunoglobulin heavy chain (IgH) repertoires. *eLife* **4**, e09083. <https://doi.org/10.7554/eLife.09083>.
- Yuan, J., Nguyen, C.K., Liu, X., Kanellopoulou, C., and Muljo, S.A. (2012). Lin28b reprograms adult bone marrow hematopoietic progenitors to mediate fetal-like lymphopoiesis. *Science* **335**, 1195–1200. <https://doi.org/10.1126/science.1216557>.

STAR★METHODS

KEY RESOURCES TABLE

REAGENT or RESOURCE	SOURCE	IDENTIFIER
Antibodies		
APC-Cy7 anti-mouse B220 (ra3-6B2)	Biolegend	Cat# 103224; RRID# AB_313007
APC anti-mouse B220 (ra3-6B2)	Biolegend	Cat# 103212; RRID# AB_312997
PE-Cy5 anti-mouse B220 (ra3-6B2)	Biolegend	Cat# 103210; RRID# AB_312995
Biotin anti-mouse B220 (ra3-6B2)	Biolegend	Cat# 103203; RRID# AB_312989
PE-Cy5 anti-mouse CD11b (M1/70)	Biolegend	Cat# 101210; RRID# AB_312793
APC anti-mouse CD138 (281-2)	BD biosciences	Cat# 558626; RRID# AB_1645216
BV605 anti-mouse CD138 (281-2)	BD biosciences	Cat# 563147; RRID# AB_2721029
BV605 anti-mouse CD150 (TC15-12F12.2)	Biolegend	Cat# 115927; RRID# AB_11204248
BV786 anti-mouse CD19 (1D3)	BD biosciences	Cat# 563333; RRID# AB_2738141
BV650 anti-mouse CD19 (6D5)	Biolegend	Cat# 115541; RRID# AB_11204087
PE-Cy7 anti-mouse CD23 (B3B4)	Biolegend	Cat# 101613; RRID# AB_2103037
PE-Cy7 anti-mouse CD24 (M1/69)	Biolegend	Cat# 101821; RRID# AB_756047
APC anti-mouse CD38 (90)	Biolegend	Cat# 102712; RRID# AB_312933
FITC anti-mouse CD38 (90)	Biolegend	Cat# 102705; RRID# AB_312926
PE-Cy5 anti-mouse CD3e (145-2C11)	Biolegend	Cat# 100310; RRID# AB_312675
Biotin anti-mouse CD3e (145-2C11)	Biolegend	Cat# 100304; RRID# AB_312669
FITC anti-mouse CD43 (S7)	BD Pharmingen	Cat# 553270; RRID# AB_394747
BV605 anti-mouse CD43 (S7)	BD biosciences	Cat# 747726; RRID# AB_2872201
PE anti-mouse CD43 (S7)	BD biosciences	Cat# 561857; RRID# AB_394748
FITC anti-mouse CD45.1 (A20)	Biolegend	Cat# 110706; RRID# AB_313495
PE-Cy7 anti-mouse CD45.1 (A20)	Biolegend	Cat# 110730; RRID# AB_1134168
APC anti-mouse CD45.2 (104)	BD Pharmingen	Cat# 561875; RRID# AB_1645215
PE-Cy7 anti-mouse CD45.2 (104)	Biolegend	Cat# 109829; RRID# AB_1186103
APC-Cy7 anti-mouse CD48 (HM48-1)	Biolegend	Cat# 103431; RRID# AB_2561462
BV421 anti-mouse CD5 (53-7.3)	BD biosciences	Cat# 562739; RRID# AB_2737758
PE anti-mouse CD5 (53-7.3)	Biolegend	Cat# 100607; RRID# AB_312736
APC-Cy7 anti-mouse CD73 (TY/11.8)	Biolegend	Cat# 127231; RRID# AB_2800626
BV421 anti-mouse CD80 (16-10A1)	Biolegend	Cat# 104725; RRID# AB_10900989
APC anti-mouse CD93 (AA4.1)	Biolegend	Cat# 136509; RRID# AB_2275879
BV421 anti-mouse CD93 (AA4.1)	BD biosciences	Cat# 747716; RRID# AB_2872195
PE-Cy7 anti-mouse CD95 (Jo2)	BD biosciences	Cat# 557653; RRID# AB_396768
BV421 anti-mouse C-Kit (2B8)	BD biosciences	Cat# 562609; RRID# AB_11154585
APC anti-mouse C-Kit (2B8)	Biolegend	Cat# 105812; RRID# AB_313221
AF-488 anti-mouse EPCAM (G8.8)	Biolegend	Cat# 118210; RRID# AB_1134099
APC anti-mouse EPCAM (G8.8)	Biolegend	Cat# 118213; RRID# _1134105
Efluor-450 anti-mouse Epcam (G8.8)	eBioscience	Cat# 48-5791-82; RRID# AB_10717090
BV421 anti-mouse Flt3 (A2F10.1)	BD biosciences	Cat# 562898; RRID# AB_2737876
Pacific Blue anti-mouse GL7 (GL-7)	Biolegend	Cat# 144613; RRID# AB_2563291
Efluor450 anti-mouse GL7 (GL-7)	Invitrogen	Cat# 48-5902-82; RRID# AB_10870775
PE-Cy5 anti-mouse Gr1 (RB6-8C5)	Biolegend	Cat# 108410; RRID# AB_313375
Biotin anti-mouse Gr1 (RB6-8C5)	Biolegend	Cat# 108404; RRID# AB_313369
APC anti-mouse IgA (mA-E61)	Thermo Fisher	Cat# 17-4204-80; RRID# AB_2848294
FITC anti-mouse IgA (mA-E61)	Thermo Fisher	Cat# 11-4204-81; RRID# _465221
PE anti-mouse IgA (mA-E61)	Thermo Fisher	Cat# 12-4204-82; RRID# AB_465917

(Continued on next page)

Continued

REAGENT or RESOURCE	SOURCE	IDENTIFIER
Biotin anti-mouse IgA	Southern Biotech	Cat# 1040-08; RRID# AB_2794374
Goat anti-mouse IgA-HRP	Southern Biotech	Cat# 1040-05; RRID# AB_2714213
Goat anti-mouse IgA unlabelled	Southern Biotech	Cat# 1040-01; RRID# AB_2314669
FITC anti-mouse IgA (C10-3)	BD biosciences	Cat# 559354; RRID# AB_397235
BV605 anti-mouse IgD (11-26c.2a)	Biolegend	Cat# 405727; RRID# AB_2562887
BV605 anti-mouse IgD (11-26c)	Invitrogen	Cat# 48-5993-82; RRID# AB_1272202
AF-488 anti-mouse IgG	Jackson	Cat# 712-545-150; RRID# AB_2340683
FITC anti-mouse IgM (II/41)	BD biosciences	Cat# 553437; RRID# AB_394857
PE-Cy7 anti-mouse IgM (RMM-1)	Biolegend	Cat# 406513; RRID# AB_10640069
Efluor-660 anti-mouse Ki67 (SolA15)	Invitrogen	Cat# 50-5698-82; RRID# AB_2574234
PE-Cy7 anti-mouse PD-L2 (TY25)	Biolegend	Cat# 107213; RRID# AB_2728122
PE-Cy7 anti-mouse Sca1 (D7)	Biolegend	Cat# 108114; RRID# AB_493596
BV421 anti-mouse TACI (8F10)	BD biosciences	Cat# 742840; RRID# AB_2741091
Biotin anti-mouse Ter119 (TER-119)	Biolegend	Cat# 116204; RRID# AB_313704
PE-Cy5 anti-mouse Ter119 (TER-119)	Biolegend	Cat# 116210; RRID# AB_313711
Bacterial and virus strains		
Lentiviral barcoding library (LV-GFP-lib)	Laboratory of D.Bryder	Lu et al., 2011
ECw murine Rotavirus	Laboratory of K.Lahl	Burns et al., 1995
Chemicals, peptides, and recombinant proteins		
7-AAD	Sigma-Aldrich	Cat# SML1633-1ML
Marina Blue Ptc DOPC/CHOL Liposomes	Formumax	Cat# F60103F-MB
Fluorescein DHPE DOPC/CHOL Liposomes	Formumax	Cat# F60103F-F
Efluor-450 Streptavidin	eBioscience	Cat# 48-4317-82
Tamoxifen	Sigma-Aldrich	Cat# T5648
Peanut Oil	Sigma-Aldrich	Cat# P2144
Progesterone	Sigma-Aldrich	Cat# P3972
Bortezomib	Cell Signaling technology	Cat# 2204
Dimethyl Sulfoxide (DMSO)	Sigma-Aldrich	Cat# D5879-100ML
Ampicillin	Sigma-Aldrich	Cat# A9518-5G
Neomycin	Sigma-Aldrich	Cat# N1876-25G
Vancomycin	Sigma-Aldrich	Cat# PHR1732
Metronidazole	Sigma-Aldrich	Cat# M3761-5G
Sucrose	Sigma-Aldrich	Cat# 84097-250G
Sodium bicarbonate (NaCHO ₃)	Sigma-Aldrich	Cat# S5761-500G
Ovalbumin	Sigma-Aldrich	Cat# A5503-10G
Cholera Toxin	BioNordika	Cat# 19654
PBS	Cytiva	Cat# SH30028.02
HBSS	Fisher Scientific	Cat# 14175-053
Bovine Serum Albumin	Fisher Scientific	Cat# AM2616
UltraPure 0.5 EDTA, pH 8.0	Life Technologies	Cat# 15575-038
HEPES Buffer Solution 1M	Fisher Scientific	Cat# 15630-056
Fetal Bovine Serum	Fisher Scientific	Cat# 15605-639
RPMI 1640	Fisher Scientific	Cat# 21875-091
Sodium Pyruvate	Fisher Scientific	Cat# 11360070
Liberase TM	Roche	Cat# 05401119001
DNase I	Roche	Cat# 10104159001
Rotavirus-like particles (VLP2/6) containing RV VP2 and VP6 bound to GFP	Laboratory of K.Lahl	Charpillienne et al., 2001
FITC PNA	Vector Labs	Cat# FL-1071

(Continued on next page)

Continued

REAGENT or RESOURCE	SOURCE	IDENTIFIER
AntigenFix	Diapath	Cat# P0014
O.C.T. compound	Tissue-Tek	N/A
ProLong Gold	Molecular Probes	Cat# P10144
Sytox Blue	Thermo Fisher	Cat# S34857
RNAzol	Sigma-Aldrich	Cat# R4533
LPS	Sigma-Aldrich	Cat# L2880
Mouse TGF- β	R&D Systems	Cat# 7666-MB-005
Mouse BAFF	R&D Systems	Cat# 8876-BF-010
TMB substrate	Mabtech	Cat# 3651-10
β -Mercaptoethanol	Sigma-Aldrich	Cat# M6250-10ML
Microbeads anti-mouse CD138	Miltenyi	Cat# 130-098-257
Critical commercial assays		
Nextera XT kit	Illumina	FC-131-1024
SMARTScribe Reverse Transcriptase kit	Clontech Takara	Cat# 39537
MiSeq V3 600c paired-end sequencing kit	Illumina	Cat# MS-102-3003
Deposited data		
VDJ-sequencing data	This paper	Zip File
Experimental models: Organisms/strains		
<i>Cd79a^{tm3(cre/ERT2)}</i>	Laboratory of M.Reth	Hobeika et al., 2015 JAX # 033026
<i>Fgd5^{ZsGreen(cre/ERT2)}</i>	In-house breeding	Gazit et al., 2014 JAX # 027789
<i>Rosa26^{LoxP-Stop-Lox-tdTomato}</i>	In-house breeding	JAX # 007909
Oligonucleotides		
Template Switching Oligonucleotide (TSO)	IDT	5'/5BiosG/AAGCAGTGGTArUCAACGC AGAGrUTCAGTGrGrG-3'
IgHM Reverse Primer	IDT	5'CTGATACCCTGGATGACTTC-3'
TSO amplification Forward Primer	IDT	5'TCGTCGGCAGCGTCAGATGTG TATAAGAGACAGAAGCAGTGGTATC AACGCAGAGT-3'
IgHM Reverse Primer (with Illumina adaptor)	IDT	5'GTCTCGTGGGCTCGGAGATGTGTA TAAGAGACAGGGAAGACATTTGGGA AGGACTGACT-3'
IgHA Reverse Primer	IDT	5'GGTTATATCCTTCCCACTC-3'
IgHA Reverse Primer (with Illumina adaptor)	IDT	5'GTCTCGTGGGCTCGGAGATGTGTATAA GAGACAG-GGTAGATGGTGGGATTC TCGCAGA-3'
Software and algorithms		
R	The R Project for Statistical Computing	https://www.r-project.org
Change-O	Immcantation Portal	https://changeo.readthedocs.io/en/stable/#
Alakazam	Immcantation Portal	https://alakazam.readthedocs.io/en/stable/
SHazaM	Immcantation Portal	https://shazam.readthedocs.io/en/stable/
Prism 9	GraphPad	https://www.graphpad.com/
Flowjo	Flowjo	https://www.flowjo.com
Other		
High affinity membrane plates	Millipore	Cat# MSP410
Cell Strainer 40 μ M	Fisher Scientific	Cat# 11517532
Cell Strainer 100 μ M	Fisher Scientific	Cat# 11587522

RESOURCE AVAILABILITY

Lead contact

Further information and requests for resources and reagents should be directed to and will be fulfilled by the lead contact, Joan Yuan (joan.yuan@med.lu.se).

Materials availability

This study did not generate new unique reagents.

Data and code availability

- The processed VDJseq results are deposited as a supplementary zip file ([Data S1](#)) to this paper.
- Any additional information required to reanalyze the data reported in this paper is available from the [lead contact](#) upon request.

EXPERIMENTAL MODEL AND SUBJECT DETAILS

Animals

Mb1Cre^{ERT2} mice (JAX 033026 *Cd79a^{tm3(cre/ERT2)}*) ([Hobeika et al., 2015](#)) and *Fgd5Cre^{ERT2}* mice (JAX 027789 *Fgd5^{ZsGreen(cre/ERT2)}*) ([Gazit et al., 2014](#)) were individually crossed with *R26^{fl-STOP-Tom}* mice (JAX 007909 *Rosa26^{LoxP-Stop-Lox-tdTomato}*) ([Madisen et al., 2010](#)) to generate time-stamping mice. All mice were bred on a C57BL/6 background and used at 12–16 weeks of age (unless specified). Both female and males were used for these study and experiments were performed on groups of at least 3 mice. All animal breeding and procedures were performed in accordance with ethical permits approved by the Swedish Board of Agriculture (M52-15, 9798-19 and 04525-17).

METHOD DETAILS

Tamoxifen induction

For induction of *Mb1Cre^{ERT2}* mediated lineage tracing Tam (Sigma-Aldrich cat #T5648) was dissolved in peanut oil (Sigma-Aldrich, cat# P2144) at 10mg/ml and given in a single dose either via intraperitoneal (i.p.) injection (day 19 and older) or fed orally (day 10 and younger) for a final dosage of 50 mg/kg. For fetal induction, E17.5 pregnant dams were given a mix of Tam and Progesterone (Sigma-Aldrich, cat# P3972) at a final concentration of 50 and 25 mg/kg respectively by oral gavage. For *Fgd5Cre^{ERT2}* mediated lineage tracing, 5-week-old mice received Tam containing food for 16 weeks as described previously ([Säwen et al., 2018](#)).

Bortezomib treatment

BZ treatment was performed on 12–16 weeks old d19 time-stamped mice by two 20 μ g i.p. injections on consecutive days as previously described ([Lindner et al., 2012](#)). BZ (Cell Signaling technology, cat#2204) was dissolved in DMSO at a concentration of 1 mM.

Antibiotics treatment

The following antibiotics were simultaneously administered via drinking at water during the indicated period of time: Ampicillin (1mg/mL, Sigma-Aldrich, #A9518-5G), Neomycin (1mg/mL, Sigma-Aldrich, #N1876-25G), Vancomycin (0.5 mg/mL, Sigma-Aldrich, #PHR1732) and Metronidazole (0.5 mg/mL, Sigma-Aldrich, cat#M3761-5G). Antibiotics containing water was supplemented with sucrose (10mg/mL, Sigma-Aldrich, cat#84097-250G) and changed twice a week.

Oral immunization with ovalbumin

Mice were gavaged with 200 μ l of 3.5% NaCHO₃ solution 20 minutes prior to immunization to neutralize gastric acid. Oral immunization was performed by administering 1mg Ovalbumin (Sigma, cat#A5503-10G) and 10 μ g Cholera Toxin (BioNordika, cat#19654) as adjuvant in a total volume of 200 μ l PBS by oral gavage. Oral immunization was repeated weekly for three consecutive weeks. Control group received PBS only.

Organ harvesting and flow cytometry

Single cell suspension from BM and spleens were subjected to red blood cell lysis and filtered. Peritoneal cavity lavage was performed using 10 mL FACS buffer (HBSS supplemented with 0.5% BSA and 2 mM EDTA). SI-LP single cell suspensions were isolated as described previously ([Johansson-Lindbom et al., 2005](#)). Briefly, intestinal content was flushed out with cold HBSS supplemented with 15 mM Hepes. Peyer's patches were excised from the SI-LP and processed into single cell suspension by mashing through 40 μ m filters. SI-LP was incubated twice with HBSS containing 2 mM EDTA, 15 mM Hepes, 2% FBS at 37 °C and digested in RPMI with 10% FBS, 10 mM Hepes, 1mM Sodium Pyruvate, 50 μ M beta-mercaptoethanol, Liberase TM, (0.3 Wünsch/mL, Roche cat# 05401119001) and DNase I (30 μ g/mL, Roche cat#10104159001) for 30–40 minutes at 37 °C on a magnetic stirrer. Antibody staining was performed in FACS buffer at a density of maximum 1×10^7 cells/100 μ l volume for 20 min at 4 °C. Lineage panel used for FACS: Ter119, Gr1, CD3. For the detection of RV specific B cells, cell suspension were first incubated for 45 minutes

with viral like particles (VLP) containing RV VP2 and VP6 bound to GFP prior to surface staining. Antibodies are detailed in the [key resources table](#). All FACS experiments were performed at the Lund Stem Cell Center FACS Core Facility (Lund University) on FACS Aria III, FACS Aria IIu, LSRFortessa, LSRFortessa-X20 and LSRII instruments (Becton Dickinson).

Immunofluorescence staining and confocal microscopy

Tissues were fixed for 1 hour in AntigenFix (Diapath), dehydrated overnight in a 35% sucrose solution and frozen in O.C.T. compound (Tissue-Tek). Tissue sections (20 μ m) were cut with a cryostat (Leica CM1950), rehydrated in PBS for 10 min and then blocked for 1 hour at room temperature with blocking solution (PBS containing saponin (0.5 %), FBS (2 %), BSA (2 %) and donkey serum (2 %)). For staining, sections were incubated overnight at 4 °C with the indicated antibodies. Stained sections were washed in PBS, mounted in ProLong Gold (Molecular Probes) mix with Sytox Blue (ThermoFisher) and visualized with a Zeiss LSM 780 confocal microscope using online fingerprint mode. Images were analysed using Adobe Photoshop 2020.

Lentiviral barcoding

LSK cells (Lin⁻ Sca1⁺ cKit⁺) were sorted from E14.5 fetal liver and transduced with Barcode-GFP-LV as previously described (Kris-tiansen et al., 2016, 2017). Briefly, the equivalent of 10000 sorted LSKs were transplanted per recipient 12h following *ex vivo* transduction. Lineage panel used for sorting was Gr1–Ter119–CD3–B220–. 16–20 weeks after transplantation, the indicated GFP⁺ mature immune cell subsets were FACS sorted and analyzed for barcode content. Samples were indexed using Nextera XT kit (Illumina) and sequenced using the Illumina NextSeq platform (Illumina). Barcode analysis was performed as previously described and barcode read frequency correlation was assessed for overlapping barcodes.

VDJ sequencing and analysis

VDJseq on cDNA was performed as previously described (Vanhee et al., 2019). Briefly, total RNA was extracted with RNAzol (Sigma-Aldrich, # R4533) and subjected to template-specific cDNA synthesis and template switching reverse transcription (SMARTScribe Reverse Transcriptase kit; Clontech Takara). A total of 2 ng of amplified cDNA was indexed (Nextera XT indexing kit; Illumina) and sequenced by using the MiSeq V3 600c paired-end sequencing kit (Illumina). [Tables S1](#) and [S2](#) contain information on number of cell sequenced, total number of reads and number of clones identified.

All analyses were performed using R version 3.2.1 (2015) and R version 3.5.2 (2018) (R Core Team; www.R-project.org/) and the ChangeO, Alakazam and Shazam packages from the Immcantation toolkit (Gupta et al., 2015). Clones were defined by collapsing sequences sharing identical V_H, D_H, J_H segment usage and CDR_{H3} nucleotide sequence. For the assignment of clonal families, clones were grouped by identical V_H and J_H segment usage, junction length and a Hamming distance of 0.1 using the DefineClones.py function of Change-O v1.0.0. Hamming value was determined by manual inspection of the distance to nearest sequence neighbor distribution using Shazam v1.0.2. For each sequence, germline sequences were reconstructed using the CreateGermlines.py function of Change-O v1.0.0 (Gupta et al., 2015). Processed VDJseq and CDR_{H3} data are supplied in supplemental zip file ([Data S1](#)).

Cell cultures

Sorted Tom⁺ and Tom⁻ B cells were cultured for 5 days at 37 °C and 5% CO₂ with the addition of LPS (50ug/mL, Sigma-Aldrich, #L2880), TGF- β (2 ug/mL, R&D Systems, #7666-MB-005) and BAFF (100ng/mL, R&D Systems, # 8876-BF-010) to promote IgA switching. PerC B cells were seeded at a density of 2.5 x 10⁴ cells/mL, splenic B cells at 1.25 x 10⁵ cells/mL.

ELISPOT assays

High affinity membrane plates (Millipore MSP410) were activated for 1 minute with 35% ethanol and coated with goat-a-mouse IgA (4ug/mL) for the detection of total IgA. Commensal ELISPOT assays were roughly based on Rojas et al. (2019). Briefly, plates were coated with heat killed fecal matter from adult Rag1KO mice (1mg/ml). Plates were blocked the next morning with 10% FBS/RPMI (Sigma) for at least 2 hrs. Sorted cells were cultured for 12–16h at 37 °C. Plates were then washed and incubated overnight at 4 °C with HRP conjugated IgA antibodies. After washing 5 times with PBS, TMB substrate (Mabtech, #3651-10) was added and plates incubated in the dark for 8 minutes or until spots were visible. Images and spot counting was performed using the ELISPOT reader IRIS (Mabtech).

Rotavirus stock preparation

Virulent wild type EC strain of RV stock were prepared by orally infecting d5 pups. The pups were sacrificed after two days of infection upon which small intestines were harvested. Tissues were lysed and supernatant from homogenate used for infection.

Rotavirus infection

Adult mice (12–16 wks of age) were infected by 3*10³ DD50 ECw virus in 100 μ l volume orally. Neonatal mice were infected with 1.5*10³ DD50 ECw virus in 50 μ l volume orally on d5. The mice were sacrificed at the indicated times post infection and the SI-LP and BM PCs were harvested for FACS analysis.

QUANTIFICATION AND STATISTICAL ANALYSIS

Statistical analysis

Statistical analyses were performed in Graphpad Prism 9. Tests for statistical significance are described in figure legends for the relevant graphs.